JOURNAL OF GEOPHYSICAL RESEARCH, VOL. 113, D01202, doi:10.1029/2007JD008550, 2008

Haboob dust storms of the southern Arabian Peninsula

Steven D. Miller,[1,2] Arunas P. Kuciauskas,[1] Ming Liu,[1] Qiang Ji,[3] Jeffrey S. Reid,[1] Daniel W. Breed,[4] Annette L. Walker,[1] and Abdulla Al Mandoos[5]

Received 15 February 2007; accepted 11 May 2007; published 12 January 2008.

[1] The Arabic word "haboob," meaning "strong wind," describes a weather phenomenon characterized by immense walls of blowing sand and dust. Common to many parts of the Middle East, northern Africa, and the southwestern United States, haboobs are spawned by strong mesoscale downdrafts, making their prediction by coarse-grid numerical models difficult in comparison to dust forced by synoptic-scale dynamics. The United Arab Emirates Unified Aerosol Experiment (UAE^2), an extensive field program conducted over the southeastern Arabian Peninsula during the summer of 2004, provided a unique opportunity to observe the haboob activity common to this region by way of a large assortment of satellite, radar, lidar, and meteorological station network observations. Here, we present results based on the UAE^2 data set which add insight to the formation processes, multiscale structure, and transient behavior of haboobs as well as their potential importance to the regional aerosol burden. Satellite imagery and surface radar data assisted in the interpretation of highly dynamic storm evolution and outflow interactions. An idealized model of haboob dust production, parameterized by the strength and duration of the downburst, suggested that haboobs could be responsible for a nonnegligible component of the regional-scale total dust production (up to 30% over a 1000 $\times$ 1000 km domain).

Citation: Miller, S. D., A. P. Kuciauskas, M. Liu, Q. Ji, J. S. Reid, D. W. Breed, A. L. Walker, and A. A. Mandoos (2008), Haboob dust storms of the southern Arabian Peninsula, *J. Geophys. Res.*, *113*, D01202, doi:10.1029/2007JD008550.

1. Introduction

[2] Dust storms represent an important source of global atmospheric aerosol particles [*Westphal et al.*, 1988; *Prospero*, 1999]. They occur when strong winds scour the land surface, lifting microscopic fragments of it into the atmosphere through a mechanical process referred to as deflation. The most significant dust storms in terms of total mass lifting, spatial extent and duration originate from powerful, sustained, synoptic-scale (i.e., 100–1000 km) winds associated with the post-frontal regime of midlatitude baroclinic systems, terrain-locked flow patterns (e.g., Shamaal winds [*Babikir*, 2004]), and barotropic easterly waves. However, various forcing mechanisms operating on the microscale to mesoscale (i.e., 1–100 km) also produce significant dust events. A noteworthy example is the evaporatively driven cold pool outflow formed by mature-phase convective cloud systems, responsible for a class of dust storm better known across the Middle East as the haboob [e.g., *Sutton*, 1925; *Lawson*, 1971; *Membery*, 1985]. Haboobs occur most often across the major deserts of Southwest Asia, Africa [*Knippertz et al.*, 2007; *Williams et al.*, 2007], and Australia [*Mctainsh et al.*, 2005] and are tied closely to the local climatology for convective activity in these regions, forming predominantly during the spring and summer months when strong solar insolation combines with influxes of monsoonal moisture to spawn powerful storms. A similar summertime monsoonal pattern leads to moderate haboob production across the arid parts of the southwestern United States [e.g., *Riley*, 1931; *Idso et al.*, 1972; *Chen and Fryrear*, 2002]. In addition, the susceptibility of surfaces to wind erosion increases during periods of extreme drought [*McCauley et al.*, 1981].

[3] Only recently have scientists begun to recognize the many teleconnections linking locally forced dust events to the global aerosol budget and, by extension, to the important interactive, or "feedback," roles played by aerosol species in the climate system. For example, we now understand that dust represents an important global-scale coupling between the lithosphere and (1) the atmosphere (via direct radiative heating/cooling of the atmospheric column [e.g., *Sokolik and Toon*, 1996; *Sokolik et al.*, 1998], the first aerosol indirect effect on cloud albedo [*Twomey*, 1974], and higher-order aerosol indirect effects impacting precipitation efficiency, cloud lifetime, and cloud thickness [*Albrecht*, 1989; *Pincus and Baker*, 1994]), (2) the biosphere (by supplying phosphate-rich nutrients to the

[1]Satellite Meteorological Applications Section, Marine Meteorology Division, Naval Research Laboratory, Monterey, California, USA.
[2]Now at Cooperative Institute for Research in the Atmosphere (CIRA), Colorado State University, Fort Collins, Colorado, USA.
[3]Earth System Science Interdisciplinary Center, University of Maryland, College Park, Maryland, USA.
[4]National Center for Atmospheric Research, Boulder, Colorado, USA.
[5]Department of Atmospheric Studies, Ministry of Presidential Affairs, Abu Dhabi, United Arab Emirates.

0148-0227/08/2007JD008550$09.00

Amazon rain forests [*Swap et al.,* 1992], increasing the mortality of coral reef ecosystems [e.g., *Prospero and Nees*, 1986], and impacting respiratory health [*Prospero*, 1999]), and (3) the cryosphere (e.g., through the acceleration of snow/ice melting by deposition of absorptive dust upon alpine snowpacks [*Flanner and Zender*, 2006; *Painter et al.*, 2007]). The strong linkage between the above processes and important branches of the Earth's hydrologic cycle (and hence coupling the lithosphere to the hydrosphere), particularly with respect to cloud and precipitation processes, makes the study of all aerosol sources essential for building a comprehensive understanding of Earth's current and future climatic states.

[4] The potential regional-scale impacts of dust lifted by the ensemble of haboobs occurring over the course of a season should not be dismissed. While originating as isolated mesoscale events (i.e., occurring on the meso-β scale of 20–200 km, as defined by [*Orlanski*, 1975]), haboobs may expand to the meso-α scale (200–2,000 km) and quite possibly to the synoptic (2,000–10,000 km) scale, broadcasting substantial amounts of dust a great distance from the source. For example, the origin of a dust/haze event reported by [*Gillies et al.*, 1996]) in Mali, West Africa was traced back via parcel trajectories to a convective system that occurred 28 hr earlier and some 500 km away.

[5] The time series of satellite imagery shown in Figure 1 illustrates the important concept of long-range transport potential by haboobs. Here, imagery from Meteosat-5, Moderate Resolution Imager/Spectroradiometer (MODIS), and Advanced Very High Resolution Radiometer (AVHRR) satellites form a multisensor chronology of a haboob at various stages in its development. In the first two panels of Figure 1, a line of late afternoon thunderstorms crossing over eastern Syria (with Meteosat-5 retrieved cloud top heights exceeding 10 km) has produced a strong gust front with accompanying dust toward the southeast and into Iraq. The cloud heights were obtained by matching satellite 11 μm brightness temperatures with temperature profiles from the Navy Operational Global Atmospheric Prediction System (NOGAPS) [*Hogan and Rosmond*, 1991] model for optically thick upper-tropospheric clouds. In the three panels to follow (labeled "NIGHT"), nighttime dust enhancements rendered from multispectral MODIS and AVHRR measurements (discussed in more detail in section 4.2) depict the incipient haboob crossing Iraq in false color as red and with a sharp demarcation at the frontal boundary. At this point, the parent storms have long dissipated and their remnants drifted to the northeast, leaving behind only the haboob within the gradually decaying outflow. The following day, the daytime MODIS dust enhancement [*Miller*, 2003] reveals the residual (fine-particle size mode) dust plume moving into northern portions of Saudi Arabia, nearly 800 km removed from its source (corresponding to a mean advance rate of 35–40 km/hr), its motion and spatial distribution governed increasingly by its entrainment within the environmental flow.

[6] Of equal importance to the broad-scale and long-term influence of dust storms are their immediate impacts on the local environment. Haboobs are characterized by sudden and intense horizontal gradients in atmospheric turbidity; visibility is reduced to perhaps a few meters in only a matter of seconds as the quite literal "wall of dust" crosses over. *Sutton* [1925] suggests average heights of these dust walls to be between 1 and 2 km. Strong winds behind the front carry large and potentially damaging sand particles with diameters from 50 μm to several mm through the processes of creeping (or rolling/skidding of large particles across the land surface) and saltation (intermittent lifting and deposition). The mass of material transported by haboobs is deceptively large. In northern and central Sudan, *Sutton* [1925] reports sand drifts as high as 5 meters that had accumulated over a two month period during the haboob season, while *Chen and Fryrear* [2002] estimate a horizontal mass flux of nearly 85 metric tons per square km per hr for a single haboob event. Naturally, haboobs pose a serious hazard to aviation due their adverse impacts to pilot visibility and equipment (sand particles dull propellers and turbine engine blades, and clog air filtration systems). Reports of the 1980 U.S. hostage rescue mission in Iran, in which a Navy helicopter collided with a C-130 aircraft under conditions of heavy dust, included references to in-flight encounters with haboobs which may have played a direct role in visibility impairment.

[7] Dust storms of the kind depicted in Figure 1, however substantial, may very well be missed altogether by numerical weather prediction models owing to a variety problems associated with (1) forecasting convection under conditions of weak synoptic-scale forcing [e.g., *Isidora and Gallus*, 2004], (2) unavailability of high spatial resolution information characterizing the environmental state, (3) inefficient coupling between nested grid scales [e.g., *Bernardet et al.*, 2000], and (4) limitations in the explicit moist physics for producing the requisite evaporatively driven downburst characteristics. As a result, haboobs have traditionally been relegated to the nowcasting (i.e., short-term forecasts on the order of hours) domain. Perhaps due to difficulties in both prediction and representation, their generally remote nature (occurring primarily in sparsely inhabited desert climates), and being of perceived secondary importance in terms of aviation hazards to the downburst itself, very little exists in the literature beyond a handful of observational studies on the specific topic of haboobs. However, to those living in or transiting through areas where haboobs occur, an improved understanding of the scale, structure, and tendencies of these rogue events is of much higher relevance. Leveraging a wealth of meteorological data available during the United Arab Emirates Unified Aerosol Experiment (UAE^2) (J. S. Reid et al., A forward to the United Arab Emirates Unified Aerosol Experiment: UAE^2, submitted to *Journal of Geophysical Research,* 2007; hereinafter referred to as Reid et al., submitted manuscript, 2007), the current study provides a first look at the haboobs of the southern Arabian Peninsula region as observed simultaneously by surface radar, a ground station network, and satellite observations.

[8] The outline of the paper is as follows. Section 2 details the physical mechanisms responsible for producing haboob dust storms and provides a review of previous theoretical and observational studies. Section 3 gives a general overview of the UAE^2 experiment and the specific observations/techniques used to detect and analyze haboobs. Selected case studies are presented in section 4, followed in section 5 by an ensemble analysis conducted with an eye toward understanding the potential role of haboobs on the regional-scale aerosol budget. Section 6

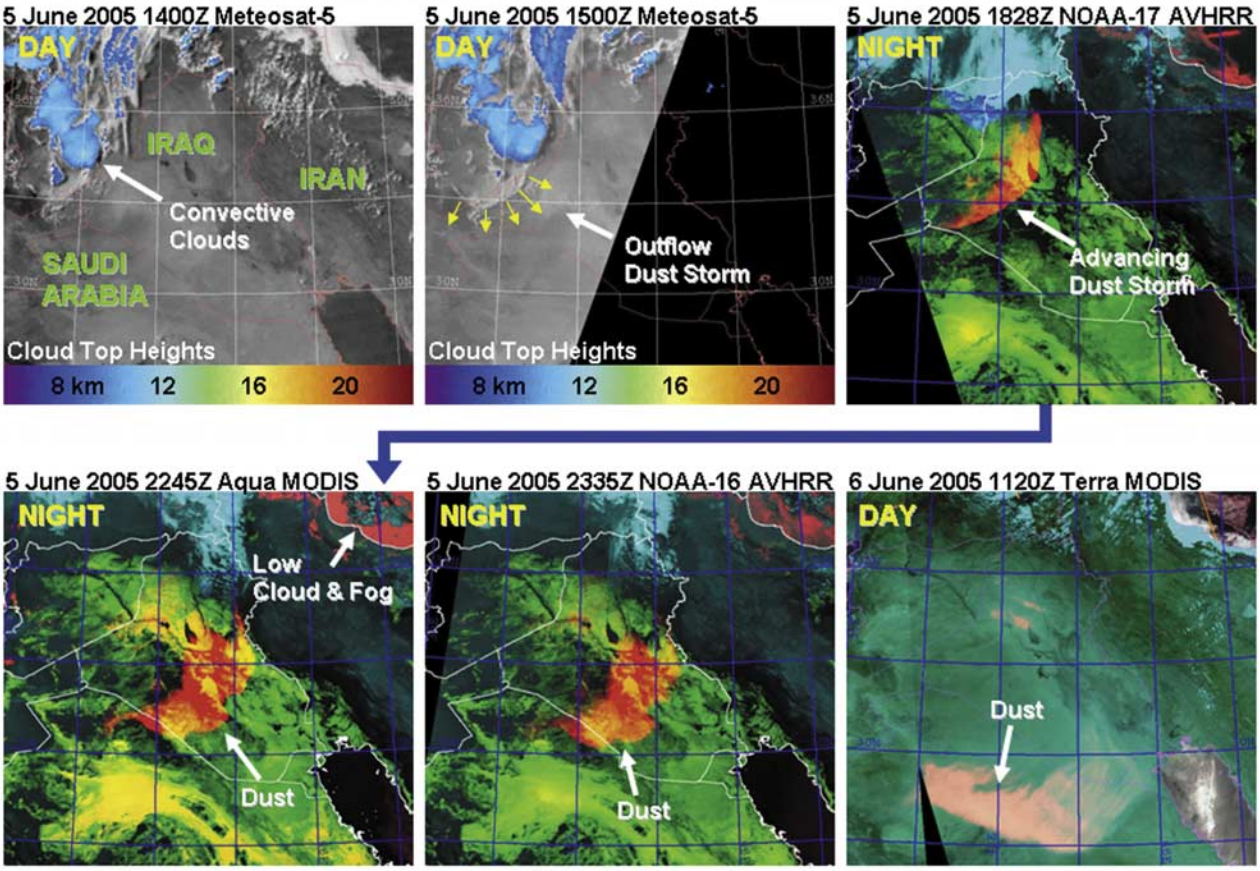

Figure 1. A multisensor (Meteosat-5, AVHRR, and MODIS, as labeled) sequence depicting the origination and ensuing trajectory of a haboob dust storm originating from a complex of thunderstorms in eastern Syria. Over the course of a day the dust front has crossed Iraq and into northern Saudi Arabia, a distance of roughly 800 km.

examines this role quantitatively through development of a simplified haboob model and its comparison against dust production from broad-scale deflation processes. A summary of the salient results and lessons learned from this study concludes the paper in section 7.

2. Background on Haboobs

[9] Originally, "haboob" applied in the most general sense to any dust raised by strong winds, regardless of the dynamics responsible for producing those winds [*Lawson*, 1971], and specifically to those events occurring across the Middle East. Over time, the term has come to refer specifically to a class of dust storms caused by evaporatively driven downdrafts (sometimes referred to in the literature as "downbursts") associated with convective clouds, and generally to any such event occurring world wide. To better understand the physical mechanisms responsible for producing haboobs, this section provides an overview of downburst characteristics (with an emphasis on dry environments), the basic requirements for deflation, and a brief review of previous haboob studies as found in the literature. Central to this discussion is a body of work from the mid-1970s to early 1980s, initiated in response to a spate of commercial airliner disasters, which resulted in significant improvements to our physical understanding and prediction of convective downbursts.

2.1. Forcing: Physical Mechanisms of Downbursts

[10] Downbursts have been studied primarily in the context of their direct impacts to aviation safety [e.g., *Fujita*, 1976; *National Transportation Safety Board*, 1983; *Wilson et al.*, 1984]. To visualize the hazard in a simplified two-dimensional way, we consider an aircraft flying through a downburst during either take-off or approach for landing. The aircraft first encounters strong headwinds as it enters the downburst outflow, followed by sudden shift to strong descending air and tail winds as it passes through the system. If the pilot adjusts for the headwind and associated enhanced lift by forcing the aircraft's nose down, this will transition quickly to a gross over-compensation in the strong descent/tail-wind (lift-depleted) region, setting the stage for potential disaster. A field program dedicated to the understanding and prediction of downbursts, conducted as part of The Joint Airport Weather Studies (JAWS) Project [*McCarthy et al.*, 1982] near Denver's Stapleton International Airport, provided a wealth of new information on their formation mechanisms and three-dimensional structure by way of three Doppler radars, two research aircraft, three rawinsonde stations, and a lightning detection system. *Fujita* [1976, 1978] defines the downburst as a strong

downdraft which induces an outburst of damaging winds exceeding 18 m s^{-1} at or near the surface. Subcategories of downbursts depending on scale are the microburst (less than 4 km outflow diameter, peak winds lasting 2–5 min) and the macroburst (having outflow diameters greater than 4 km, durations of 5–20 min, and capable of causing up to F3 intensity tornado-equivalent damage). *Wolfsen* [1983], *Caracena et al.* [1983], *Wilson et al.* [1984], and *Wakimoto* [1985] provide further distinction of between wet and dry microbursts, according to the amount of rain accompanying the period between the onset and end of high winds.

[11] Parcel theory describes and predicts the descent of a negatively buoyant air mass according to the buoyancy equation:

$$\frac{dw}{dt} = g\frac{T' - T}{T}dz - D_p, \tag{1}$$

where T' and T are the virtual temperatures of the parcel and the environment, respectively, and D_p accounts for downdraft enhancement by precipitation drag effects. By assuming steady state conditions, negligible D_p, and no horizontal advection of w, Equation (1) can be re-cast via the hydrostatic equation and ideal gas law as

$$\frac{1}{2}\left(w^2 - w_o^2\right) = -R\int_{p_o}^{p}(T' - T)\frac{dp}{p}, \tag{2}$$

where w_o and p_o are the vertical wind speed and pressure (respectively) at cloud-base, and R is the gas constant (for either moist or dry air, depending on state of the parcel in its sub-cloud descent). Equation (2) illustrates the fact a downburst's potential energy is simply the convective inhibition (CIN); the negative-area analog to the convective available potential energy (CAPE). However, the processes that determine the initial conditions necessary for production of a strong downburst reaching the surface typically are far more complex. A number of hypotheses have been proposed in the literature to describe downburst initiation, including (1) mixing of cloud-top-entrained dry air leading to local evaporation and downdrafts [*Squires*, 1958; *Emanuel*, 1981; *Caracena and Maier*, 1987], (2) precipitation drag effects [*Clark and List*, 1971], (3) downward transport of upper level horizontal momentum [*Newton*, 1950], and particularly important for dry microbursts, (4) evaporative cooling from precipitation falling into a dry sub-cloud layer [*Krumm*, 1954; *Kamburova and Ludlam*, 1966]. Regardless of what combination of mechanisms are involved aloft, the end result near the surface is a strong, localized divergent wind field pattern. The incipient gust front may be asymmetric due to (1) superposition of storm motion, (2) effects of vertical shear (e.g., rotating downdrafts as examined by *Fujita and Wakimoto* [1983] and *Weisman et al.* [1983]), (3) superposition of environmental surface winds, (4) superposition of multiple gust fronts spawned by the same storm or nearby ones, or, as mentioned above, (5) any component of upper-level momentum transported to the surface. All haboob events observed during UAE^2 demonstrated some degree of asymmetry, attributable presumably to at least one or more of the mechanisms listed above.

[12] It is important to point out that whereas all convection produces downdrafts, most do not reach the surface as downbursts and subsequent divergent gust fronts. This is because often a moist sub-cloud environment prevents them from doing so (e.g., compressional heating allows the descending parcel temperature to catch up rapidly to a moist environmental temperature lapse rate and thereby attain neutral buoyancy). Downdrafts that occur in a dry adiabatic rate environment, on the other hand, stand a better chance of reaching the surface. Given the typically dry lower atmospheric conditions of arid regions, it is perhaps by no coincidence that dry downbursts [e.g., *Braham*, 1952; *Krumm*, 1954], associated with little or no precipitation at the surface, are the variety most often associated with haboobs. Several time-dependent modeling studies [*Srivastava*, 1985; *Proctor*, 1988, 1989] outline the conditions favorable for producing a strong downdraft at the surface, including (1) dry adiabatic sub-cloud layers, (2) high rainwater mixing ratio at cloud base, and (3) small drop sizes. From JAWS data sets, *Hjelmfelt* [1987] observes a decrease in high reflectivity core intensities below cloud base due to evaporation. Parcel cooling due to evaporation of its liquid/ice water content (virga shafts) is a key mechanism for producing negative buoyancy.

[13] Also, as implied by equation (2), evaporation of precipitation into a very deep dry adiabatic sub-cloud layer (i.e., high-based cloud systems [e.g., *Rodi et al.*, 1983; *Knupp*, 1985]) can lead to a large downdraft potential energy even for relatively small negative buoyancy at any given level. As the parcel descends, it follows a moist adiabatic lapse rate until most of its water (ice) is evaporated (sublimated), and follows a dry adiabatic lapse rate thereafter. If the environmental air is also following the steep dry adiabatic lapse rate, then the downdraft parcel will never overcome its negative buoyancy through compressional heating [e.g., *Srivastava*, 1985, Figure 2]. Instead, it will remain cooler than the environment and continue unabated toward the surface. Warming due to entrainment of environmental air may reduce the final downdraft at the surface, although rotating downdrafts sometimes observed in the presence of strong environmental wind shear [*Fujita and Wakimoto*, 1983; *Weisman et al.*, 1983] are thought to inhibit the entrainment process by increasing inertial stability.

[14] Most dry microbursts reach the surface at a lower relative humidity and temperature than the environment. However, it is possible to produce warm-air downbursts if the downward momentum is sufficient to overcome the depth of a shallow low-level temperature inversion (e.g., set up by strong radiative cooling at the surface toward the evening hours). Also, since evaporation in the virga shaft increases relative humidity while descent tends to reduce it, it is possible for a ground station to observe complicated fluctuations between lower and higher relative humidity as an evolving storm complex crosses over. For a haboob observed near Phoenix, Arizona, *Idso et al.* [1972] report drops in temperature on the order of 7 °C (range 3–13 °C) and increases in relative humidity on the order of 33 to 74%. More recently, airport observations of a haboob-producing downburst that crossed Casa Grande (also in Arizona) on 6 June 2006 recorded a nearly 20 °C temperature reduction and 35% increase in relative humidity. While these cases could be the result of wet microburst activity, the UAE^2

examples to follow demonstrate that dry microbursts produce both dry and moist relative humidity anomalies as suggested by the modeling results of *Srivastava* [1985].

[15] *Kamburova and Ludlam* [1966] and *Brown et al.* [1982] explain the importance of a smaller precipitation size distribution for a given liquid water content (e.g., a high concentration of lightly rimed snowflakes as opposed to a smaller concentration of large graupel/hail) in providing more efficient evaporation to in turn produce stronger negative buoyancy. Formation of such a particle size distribution (i.e., weighted toward smaller sizes) often results from weaker updrafts. For example, *Caracena et al* [1983] note relatively weak buoyancy at low to mid levels of shallow, high-based (bases at ~500 mb) cumuli whose downdrafts produced rapidly evaporating virga shafts that then developed into significant dry microbursts. *Srivastava* [1985] confirms this tendency in numerical simulations. While the suggestion here is perhaps counterintuitive, vigorous convection is not a necessary condition for the production of strong downbursts. More important are the dry adiabatic sub-cloud environment and kind of hydrometeor involved (e.g., even small quantities of snow falling into deep, dry layers can generate strong downdrafts).

[16] While the seasonal trends of haboobs (spring/summer months, tied to increased solar insolation and, in some regions, influx of regional moisture) are well noted, less understood are their possible linkages to synoptic scale conditions. In other words, whatever the mechanism for cumulonimbi formation, be it elevated heat sources (mountain ranges or plateaus), surface wind convergence zones, or along frontal boundaries, "air mass" variety or organized, the ultimate criteria for whether these clouds produce downbursts are tied to the local environmental state, cloud/precipitation microphysical characteristics, and associated thermodynamic processes. As *Hjelmfelt* [1987] points out during the High Plains JAWS field study, there is no single characteristic cloud pattern associated with downburst production; they can form as symmetric, isolated storms (weak flow aloft), symmetric after removing the strong environmental flow, or as squall lines. This fact combined, with the typically fine space and timescales of their parent cloud systems (of order 10 km and 1 hr), make downbursts and by extension, haboobs, extremely difficult to predict.

2.2. Mechanics of Deflation

[17] The strong winds of a dry microburst do not always result in mobilization of dust. The susceptibility of a given surface to deflation depends on its vegetation cover, soil moisture, and the size, shape, and distribution of the soil particles themselves [e.g., *Gillette et al.*, 1981]. Increased vegetation and soil moisture tend to bind the surface, reducing its susceptibility to erosion by wind in comparison to barren and dry desert surfaces. Given the high spatial variability of surface types, one should expect the deflation susceptibility to vary commensurately. In many cases, extensive dust storms have been observed to originate from a few point sources such as silt-laden wadis, topographic wind-channeling (gap wind) regions, or dry lake beds where local erodibility is high. Certain desert surfaces prone to frequent wind-scouring evolve into "desert pavement," where nearly all loose material has been removed over time and only the tightly bound materials remain (hence reducing its susceptibility to further deflation). *Helgren and Prospero* [1987] show for eight observing stations in the Western Sahara that the critical wind velocity above which deflation of surface sediments occurs, also called the threshold wind speed (U_T), is highly variable (ranging from 5 to 12.5 m s^{-1}) from location to location but remains stable at any individual location. On the continental-to-global scales, *Prospero et al.* [2002] provide an atlas of dust source regions based in part on Total Ozone Mapping Spectrometer (TOMS) satellite observations and terrain data. In global and regional mineral aerosol studies dust source regions are determined by land/vegetation cover databases. The land classifications most susceptible to wind erosion are desert, shrub, grassland and bare soil. The two most commonly used databases for classifying surfaces in this way are the United States Geological Survey (USGS) Global Land Cover Characteristic (GLCC) database and the Normalized Difference Vegetation Index (NDVI) Land Surface Classification Database developed by *DeFries and Townsend* [1994]. Performance of these databases in the context of dust transport modeling is examined by *Uno et al.* [2006] and *Ginoux et al.* [2001].

[18] To account for the important roles of surface roughness and atmospheric stability (which determine the amount momentum transferred to the surface and the subsequent degree of lofting into the atmosphere), *Westphal et al.* [1988] propose a threshold on the friction velocity (u_*) as a potentially more robust alternative to U_T that is suitable for incorporation in physical transport and dispersion modeling:

$$u_* = U_s\kappa/[\ln(z_s/z_o) - \psi_m(z_s/L)], \tag{3}$$

where U_s represents a near-surface wind speed measured at level z_s, κ is the von Karman constant, and z_o, ψ_m, and L are the surface roughness length, momentum stability parameter, and the Monin-Obukhov length, respectively. For threshold velocities ranging from 5 to 11 m s^{-1} and daytime desert conditions, the corresponding threshold friction velocities range from 25 to 77 cm s^{-1}. On the basis of previous modeling work and field experiments [*Gillette and Passi*, 1988], 60 cm s^{-1} is considered a typical threshold value for the onset of deflation. Since our current understanding of deflation processes is poor [e.g., *Giles*, 2005], typically we rely on empirical relationships to capture them implicitly. Following *Westphal et al.* [1987], the source flux (in g cm^{-2} s^{-1}) of dust with particle radii between 0.1 and 80 μm produced as a function of friction velocity is parameterized as

$$F_a = 2.9 \times 10^{-14} u_*^4. \tag{4}$$

[19] The small particle component (diameters of 10 μm or less; considered important for long range transport) of the size distribution assumed for this model accounts for about 4.4% of this total mass flux. In practice this transportable fraction typically ranges from 4 to 15%, depending on size distribution assumptions and empirical studies conducted over different regions. In section 6 we will apply the above relationships along with other simplifying assumptions to a first-order estimate of haboob dust production.

[20] Once the friction winds reach sufficient intensity to initiate deflation over a given surface type, the specific behavior of dust mobilization will vary thereafter as a function of particle size and wind speed. For lighter winds, larger particles skid across the surface in a process called creeping, while smaller particles are lofted airborne for a short distance before falling back to the surface through a process called saltation. Still finer grain materials will be lifted and carried in suspension for extended distances [e.g., *McCauley et al.*, 1981; *Gillies et al.*, 1996; and *Prospero*, 1999]. Stronger winds are capable of transporting the larger particles via the saltation process. Interestingly, studies indicate that the threshold friction velocity for the smallest particles is somewhat higher than the larger diameter particles, possibly owing to the distribution of these particles in the surface layer and the dependence of binding energy on particle size (Coulomb forces [e.g., *Vogel et al.*, 2006]). The airborne residency time of dust decreases with increasing particle size due to gravitational fall-out. The observed dust particles originating from a distant source are typically found to have particle volume median diameters of about 5 μm, resulting in haze conditions [e.g., *Gillies et al.*, 1996], contrasting drastically with the brown-out/sand-blasting conditions that accompany the coarse mode (tens to hundreds of μm) distribution found in an early-stage haboob. Whereas the fine mode holds greater potential for climate (via both direct and indirect effects) and respiratory health impacts, the coarse mode presents hazardous operating conditions for all modes of transportation.

2.3. Previous Observational Studies of Haboobs

[21] While haboobs are not uncommon phenomena, their natural association with the deserts of the world means that they tend to occur more often in sparsely populated regions far removed from the meteorological observation networks required for their proper study. Perhaps it is for this reason there are so very few scientific papers written specifically on the topic of haboobs despite an extensive body of literature on their primary forcing mechanism, the downburst, as detailed above. Furthermore, most research to date has been either episodic (case study) or else entail multiyear statistics confined to a single observation site. Nevertheless, these previous studies shed important light on the morphology, content, and meteorological properties of haboobs and their associated gust frontal systems.

[22] Among the earliest published works, *Sutton* [1925] examines statistics of haboobs observed over an 8 year period in the Khartoum district of northern/central Sudan. The walls of dust associated with these storms typically exceeded 1 km in height, lasted anywhere from 30 minutes to several hours, were accompanied by strong surface winds, and were followed by rain showers 50% time in early season (May to June) and 70% in late season (July to September). Synoptically, a general warming trend and pressure fall over the course of several days preceded the observed haboob outbreaks, followed by a drop in temperature and sharp rises in pressure and relative humidity.

[23] *Lawson* [1971] revisits the haboobs of the Sudan region, noting that one particularly strong nighttime event featured a 4.5 °C drop in T over 15 min, and adding that the dust was restricted almost entirely to the cold pool region. He also notes that the speed of dust front advance was approximately half the maximum wind speed measured behind the front. This apparent contradiction may be explained by the redirection of horizontal motion into the vertical along the forward edge of a ring vortex associated with the downburst front itself [e.g., *Proctor*, 1988]. In examining the microscale structure and propagation of the haboob dust wall, Lawson draws an analogy to the density current simulations of *Simpson* [1969]. Consistent with observations, those simulations suggest that small "microlobes" of dust are pushed out ahead of the main cold pool body, expanding horizontally/vertically until they slow and eventually are overcome by new lobes surging forward.

[24] In one of the very few in situ microphysics studies, *Chen and Fryrear* [2002] provide a detailed account of a haboob event near Big Spring, Texas. Interestingly, in this case the wall of dust arrived under relatively quiescent conditions and approximately 1.5 hours ahead of the discontinuities of wind (10 m s^{-1} increase), temperature (7° C decrease), and surface pressure ($\sim$1 mb increase) associated with passage of the evaporative cold pool front. This contrasts markedly with previous reports where the dust front invariably is coupled closely with the nose of the cold pool front. Unfortunately, a time series of satellite imagery helpful in identifying and observing the location and evolution of the parent cloud system and its outflow was not included. Other ideas are presented in the context of the case studies of section 4. It becomes evident that a single ground station observation, while useful in its level of local detail, cannot provide the big picture view needed to fully understand the life cycle and structure of haboobs. In this regard, UAE^2 provided a unique opportunity to examine the problem from both local and regional scales.

3. UAE^2 Overview

3.1. Scope of Program

[25] The current work was conducted in the context of the UAE^2, a field program conducted over August to September 2004 that brought together an international group of scientists and observing system resources that represented 8 countries and 24 institutions for the common purpose of investigating the complex and diverse aerosol environment of the Arabian Gulf region. Largely unstudied to date, the region is characterized by an extremely high and chemically/microphysically complex aerosol loading due to the confluence of (1) frequent dust storms from a wide variety of surrounding sources (both local and remote), (2) smoke/pollution transported from the Indian subcontinent, and (3) locally produced industrial pollution.

[26] The principle focus of UAE^2 was on broader scale aerosol-radiation-meteorology feedbacks across the greater Southwest Asia domain. Nevertheless, it offered an unprecedented consolidation of remote and in situ sensing resources for examining mesoscale events such as haboobs. Included in the field program were instrumented aircraft, an aerosol-measurement surface network (AERONET [e.g., *Holben et al.*, 2001]), lidars, and general meteorological station networks, surface-based radar and lidar, and two heavily instrumented aerosol observation facilities. Further, the UAE Dept. of Water Resource Studies (now Dept. of Atmospheric Studies) deployed a mesonet of weather stations across the UAE. Aerosol optical depth retrievals from

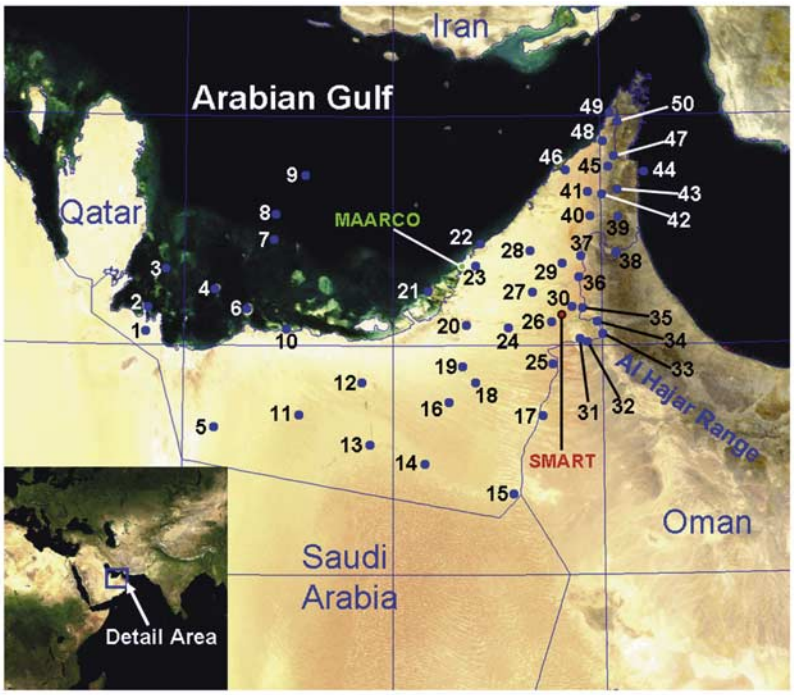

Figure 2. The UAE^2 study domain surface meteorological station network overlaid upon NASA/MODIS Blue Marble data. Refer to Table 1 for station index details.

AERONET via solar occultation measurements typically were not available for the haboob cases due to presence of neighboring convection and especially cirrus blow-off (anvils) from the parent cloud systems themselves. These upper-level clouds also tend to obscure many haboobs from the view of passive-sensor satellite observing systems. Readers interested in the details of all observing platforms and coordinated activities during UAE^2 are referred to Reid et al. (submitted manuscript, 2007). This section describes in brief the subset of systems used for the specific analysis of haboob dust storms.

3.2. Surface Observation Network

[27] The UAE mesonet consisted of 52 stations distributed across the country (biased in density toward the northeast portion of the domain), including several offshore sites. Figure 2 shows the spatial distribution of this network, with Table 1 serving as the station index key. The stations supplied temperature (T), pressure (P), relatively humidity (RH), and surface wind (W) vectors at 15 minute (time averaged) temporal resolution. A key component of the surface network for the current study was the Surface-sensing Measurements for Atmospheric Radiative Transfer (SMART) station, developed by the National Aeronautics and Space Administration (NASA) Goddard Space Flight Center (GSFC). Deployed at the Al Ain International Airport (24.26N, 55.62E, and 250 m elevation), SMART provided comprehensive mobile ground-based laboratory for measurements of global/diffuse/direct solar irradiance (broad and narrow band), global sky thermal irradiance, transmitted solar spectral radiance, emitted downwelling infrared spectral radiance, microwave downwelling sky radiance, normalized backscatter intensity, surface meteorological parameters (T, P, and RH at a sampling interval of 1 s). An important sub-component of SMART for this study was its all-sky camera, which provided visual confirmation of dust frontal passage (FROPA) and exact timing of haboobs with respect to rapid fluctuations in the meteorological parameters measured.

[28] SMART was co-located with two active sensors: a C-band (5 cm wavelength) Doppler radar operated by the Department of Civil Aviation in cooperation with UAE Department of Atmospheric Studies [see *National Center for Atmospheric Research*, 2005], and the NASA/GSFC 532 nm micropulse lidar (MPL) [*Spinhirne et al.*, 1995; *Welton et al.*, 2001]. The radar provided detailed information on the location of haboobs through measurement of backscatter from large dust particles and the strong gradient of refractive index across the mesofront. Available as plan-position indicator (PPI) scans at roughly 5 minute temporal resolution (volume scan repeat time) and up to roughly 240 km range at 500 m gate spacing, these data were useful in understanding storm evolution and the source of dust fronts crossing SMART, and particularly in circumstances of multiple gust fronts. The MPL was operated in a zenith-pointing (nonscanning) mode, providing cross sections of aerosol (including the vertical extent of haboobs) passing over the site. While lidars attenuate rapidly in the presence of optically thick cloud cover (particularly in the liquid phase), they provide an estimate of cloud base height accurate to within 75 m, information that when combined with radiosonde temperature/moisture profiles allows for estimation of downburst potential energy in the profile and hence downburst wind speed (see equation (2)).

Table 1. UAE Meteorological Station Positions Corresponding to Figure 2

Index	Station Name	Latitude, °N	Longitude, °E	Elevation, m
1	Alghweifat	24.12	51.63	69
2	Ras Musherib	24.33	51.65	22
3	Makassib	24.67	51.82	20
4	Dalma	24.49	52.29	25
5	Al Jazeera	23.29	52.29	25
6	Sir Bani Yas	24.32	52.60	143
7	Qarnen	24.93	52.85	32
8	DAS	25.15	52.87	12
9	Abu Al Bukhoosh	25.49	53.15	37
10	Alqlaa	24.15	52.98	11
11	Owtaid	23.40	53.10	180
12	Madinat Zayed	23.68	53.70	118
13	Mezaira	23.14	53.78	204
14	Hamim	22.97	54.30	126
15	Um Azimul	22.71	55.14	140
16	Bu Humrah	23.51	54.53	171
17	Alqlaa	23.39	55.42	150
18	Rezeen	23.68	54.78	123
19	Tawi Dakhnan	23.82	54.66	123
20	Alwathbah	24.18	54.70	63
21	Abu Dhabi	24.48	54.33	7
22	Ghantuat	24.89	54.84	29
23	Alsamha	24.70	54.79	35
24	Alkhazna	24.16	55.10	192
25	Alarad	23.84	55.52	212
26	Alsad	24.21	55.51	199
27	Swiehan	24.47	55.33	170
28	Saih Al Salem	24.83	55.31	105
29	Al Faqa	24.72	55.62	235
30	Al Raknah	24.34	55.71	288
31	Jabal Hafeet	24.06	55.78	1059
32	Mezyed	24.03	55.85	345
33	Alsaa	24.10	56.00	524
34	Khatam Al Shaklah	24.21	55.95	433
35	Alfoah	24.33	55.81	335
36	Alhiyar	24.60	55.78	325
37	Al Shiweb	24.78	55.80	306
38	Hatta	24.81	56.14	325
39	Al Heben	25.12	56.16	933
40	Al Malaiha	25.13	55.89	186
41	Falaj Al Moalla	25.34	55.87	120
42	Manama	25.32	56.01	217
43	Masafi	25.36	56.16	525
44	Dhudna	25.51	56.42	64
45	Tawiyen	25.56	56.07	186
46	Umm Al Quwain	25.53	55.66	20
47	Jabal Mebreh	25.65	56.13	1450
48	Wadi Al Bih	25.78	56.02	69
49	Sham	26.03	56.09	43
50	Jabal Jais	25.95	56.17	1739
–	MAARCO	24.70	54.66	10
–	SMART	24.26	55.62	250

3.3. Satellite Observation Network

[29] *Gurka* [1977] and *McCauley et al.* [1981] provide early demonstrations of how satellite remote sensing can be used to detect and track large dust storms. Sensors on board geostationary (GEO) platforms offer high time resolution useful in monitoring the formation and transport of dust, while low-earth orbiting (LEO) platforms sacrifice temporal refresh for higher spatial resolution and currently offer a greater diversity of sensors and spectral channels useful in identifying mesoscale properties and providing superior microphysical information. The duration, scale, and microphysical/macrophysical properties of haboobs make them prime candidates for monitoring by way of both GEO (mainly, tracking their parent convective complexes) and LEO (e.g., fortuitous timing of satellite overpass during an event in progress) observing systems. We are not aware of any published studies to date that make use of satellite data for the specific purpose of examining haboob-class dust storms.

[30] Complementing the surface observation network during UAE^2 was a suite of environmental satellites supplying multispectral information useful in detecting and characterizing atmospheric aerosol properties, distribution, and transport. The constellation included Meteosat-5, NASA Terra and Aqua, the Sea-viewing Wide Field-of-view Sensor (SeaWiFS), and the National Oceanic and Atmospheric Administration (NOAA) Polar-Orbiting Environmental Satellite (POES) and Defense Meteorological Satellite Program (DMSP) systems. Through coordination with the NOAA, NASA, and the Air Force Weather Agency (AFWA), the digital data sets for a total of 31 (at the time of this writing) distinct and globally distributed satellite sensors arrive at the Naval Research Laboratory in near real-time (typically less than 3 hr latency). A collection of value-added imagery products based on these data and ancillary information from numerical weather prediction models (e.g., temperature soundings for cloud height estimation) was processed in near real-time via automated scripts and hosted upon the ''Satellite Focus'' Web-based application [*Miller et al.*, 2006] to support flight operations during UAE^2 field campaign. For the specific interests of this research, Meteosat-5 data served as the primary tool for monitoring convective activity within domain, and LEO data were exploited opportunistically as mentioned above.

3.4. Observing System Synergy

[31] Haboobs possess both mesoscale and sub-mesoscale characteristics, and as such, some aspects are best captured by a surface network (e.g., dynamic, thermodynamic, and microphysical properties) while other aspects (e.g., forcing, structure, evolution, and other macrophysical properties of dust transport) are better suited to satellite analyses. In this study, both satellite data and radar cell tracking were used to identify the location and evolution of potential haboob-producing storms, and surface observations were used subsequently to confirm specific events and examine them in further detail.

[32] Despite the wealth of information available during UAE^2, there remain several limitations of the data sets to the particular topic of haboob studies. For example, wind measurements were not collected at SMART, precluding a detailed analysis of the fine-scale wind structure during the haboob crossings at Al Ain. Furthermore, station data for Al Ain were not available, leaving no direct wind speed records of any kind for this important site. The approach followed here for frontal and peak-wind analysis involved both direct (e.g., radar gust front tracking) and indirect measurements (inferring wind from T/P/RH changes) to arrive at consensus values. Fortunately, there were several stations surrounding Al Ain where wind speeds were available. Their irregular spacing limited the ability to resolve adequately the transient, nonlinear dynamics of

haboob frontal passages for some cases. Superposition of multiple gust fronts, interaction with a complex environmental flow, and positioning of stations with respect to storms producing asymmetric outflows add further complications to interpretation by producing a highly variable time series of the aforementioned meteorological parameters. Enough events occurred over the course of the study period to select cases that were isolated well-positioned with respect to the surface network. The meteorological station wind speed observations, although sampled at 1 Hz, were averaged and reported at 15 min intervals. This averaging tended to smooth the sharp wind speed and direction gradients experienced during gust front passages, and depress peak wind speeds reported (no "peak gust" values were included over these averaging periods).

[33] In terms of limitations to satellite-inferred haboob forcing (i.e., relating observations of rapidly growing convective cloud structures to incipient downburst production), it should be pointed out that cloud observations are not always the best method for identifying severe weather [e.g., *Wakimoto*, 1983] or microbursts in particular [*Brown et al.*, 1982; *Wakimoto and Bringi*, 1988]. As mentioned previously, the cirrus anvil of mature convection will often mask the low-level haboob structure from satellite's view. In other cases, the haboob dust wall extends well ahead of the anvil and is clearly evident from satellite imagery. In this case the satellite data can be used to estimate the approximate crossing times over members of the ground station network.

3.5. UAE Domain Characteristics

[34] The UAE is in a region characterized by high dust production potential, with semi-desert shrub and bare desert surface classifications and high erodibility factors (defined here as the susceptibility of soil to wind-induced detachment and transport). The geography of the region also plays an important role in determining the frequency of haboobs forced over the region. Specifically, the Al Hajar mountain range (extending along the UAE/Oman political border southeastward toward the Gulf of Oman), whose highest peaks are in the range of 1.4–1.6 km above mean sea level, represents an elevated heat source and a fairly reliable focal point for convective initiation during the summer months.

[35] The orographic forcing observed along the Al Hajar is in some ways analogous to the Colorado High Plains convection initiated in the presence of summertime monsoonal moisture advected over the Rocky Mountains, as studied during JAWS. In the case of the UAE domain, the moisture flux during preferred conditions for haboobs enters the region primarily from the Indian Ocean/Gulf of Oman waters to the east/southeast, with convection moving off the Al Hajar and reaching its mature phase (the point at which downbursts form) over the desert plains to the west. For active days examined during UAE^2, this process typically initiated around early afternoon (0900-1000 UTC; the UAE being 4 hours ahead of UTC), dissipated by the early evening (1500-1600 UTC), and consisted of roughly 4–8 distinct convective cells in the immediate vicinity of the study area.

[36] Another important mesoscale mechanism common to the UAE region is the sea breeze front (SBF). Early morning flow over the summer months is dominated by a light (typically less than 5 m s^{-1}) southerly land breeze blowing toward the relatively warmer Arabian Gulf waters to the north. Intense solar heating of the desert interior, including the Al Hajar range, forms a thermal low pressure center which typically by mid-day begins drawing in air from over the now relatively cool Arabian Gulf waters. SBFs have very strong moisture gradients, and may also lift small dust particles. Therefore they may appear as haboobs to Doppler radar systems, and care had to be taken in this analysis to match radar-observed frontal structures with satellite-observed parent convective clouds. SBFs impinging on the western and eastern slopes of the Al Hajar enhance vertical motion, triggering early-afternoon convection. In other instances the convection forms first and the outflows from these systems collide with the SBF to trigger/intensify additional convection, leading to an increasingly complicated structure of outflow boundary propagation with time until most of the activity dissipates by early evening.

4. Selected Cases

[37] The intensive observing period of UAE^2 spanned the months of August and September 2004. There were numerous days over this period when convective activity initiated over the Al Hajar range in the early afternoon hours and subsequently drifted over the desert plains of the eastern UAE due to the prevailing easterlies/south-easterlies aloft. For this research we considered station observations of haboob frontal passages from seven especially active days during UAE^2 (21 August and 3, 13–14, 17, and 22–23 September), three of which are presented here in some detail and the remainder contributing to the ensemble analysis to follow. Conveniently, the SMART station's deployment at Al Ain placed it at one of the more strategically favorable locations for encountering haboob activity.

4.1. The 3 September 2004 Case: Al Hajar Range

[38] Around 0930 UTC on 3 September 2004, convective clouds formed over the Al Hajar range ~15 km west of Alfoah (24.33N, 55.81E), near the border between the UAE and Oman. By 1000 UTC, cloud top heights for the original cells of this complex had reached 8 km, and one had initiated a downdraft outflow detectable by the Al Ain radar. This outflow was observed to intersect and subsequently intensify two additional convective cells to the northwest. These latter storms in turn produced their own downbursts which served to augment the northwestern quadrant of the original haboob (*Idso et al.* [1972] give mention to such complicating factors of multiple cells and superposition/merger of multiple dust fronts). The haboob crossed several UAE^2 designated observing stations, including SMART. The radar's high space and time resolution volume scans revealed that what had appeared to be a single convective cell from the coarse 4 km resolution satellite imagery was in fact a complex distribution of multiple high reflectivity cores having horizontal scales of ~5 km and individual life cycles of about 1 hr.

[39] Figure 3 depicts the passage of the haboob over the SMART station at Al Ain as observed by Meteosat-5, the MPL, the Al Ain radar, and the SMART all-sky camera. The Meteosat-5 1100 UTC image shows a localized area of convection with cloud tops exceeding 12 km, while the MPL data show the cloud base varying between 4.5 and

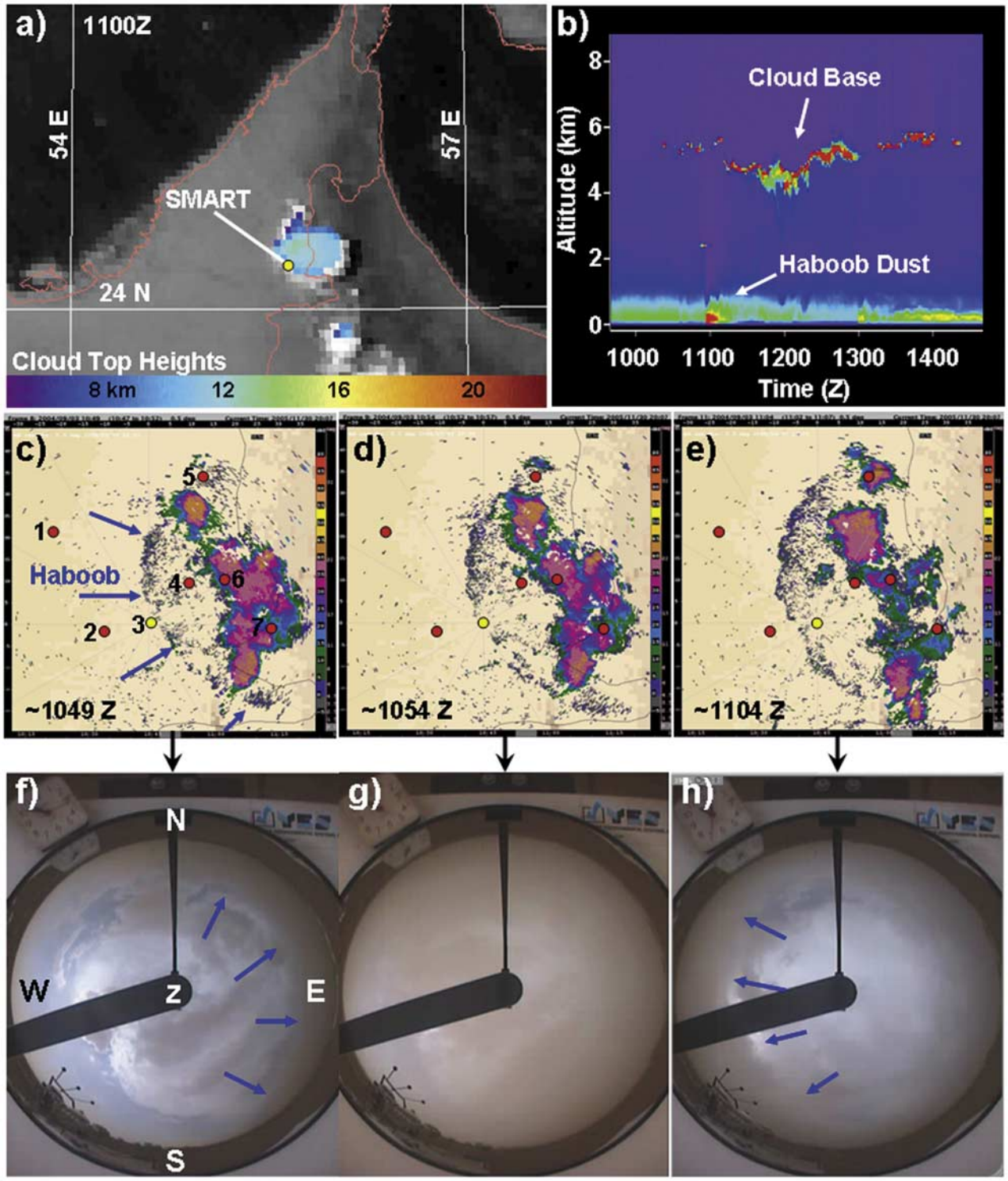

Figure 3. The 3 September 2004 haboob case as observed at Al Ain by (a) Meteosat-5, (b) the NASA MPL, (c-e) the C-band radar (yellow dot denotes Al Ain/SMART, and red dots are surrounding Met stations listed in the text; blue arrows identify haboob outflow), and (f-h) the SMART all-sky camera (N/S/E/W denote approximate compass bearings, "z" denotes local zenith, and blue arrows show approaching/receding dust) as the dust front passed over the station. MPL imagery courtesy of NASA, and radar imagery courtesy of the UAE/DAS.

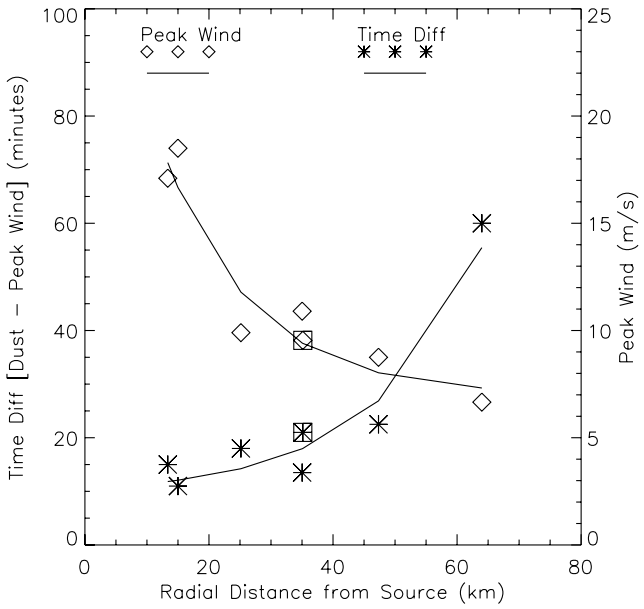

Figure 4. Trends in station-observed peak winds (diamonds) and delays between time-of-arrival for dust and peak cold pool wind speed (asterisks) plotted as a function of radial distance from the radar-estimated downburst point of origin for the 3 September 2004 haboob case. Boxed points correspond to the SMART station data. Curves are exponential fits to the data; coefficients provided in text.

5 km and the haboob dust feature reaching a height of about 500 m. For comparison, hand analysis of the closest available rawinsonde data (Abu Dhabi, 130 km to the west/northwest of Al Ain, collected at 1100 UTC) suggested a 4.1 km convective condensation level). The radar data agree with all-sky camera observations on the arrival of dust, which crossed over the station at ~1054 UTC. On the basis of samples taken at four different positions along the dust front it was determined from the radar data that the haboob was moving at approximately 10.5 m s^{-1} (37.7 km/hr), expanding from a source located ~15 km east of the Alfoah station. Meteorological observation stations located downstream of this event (i.e., in a radial sense, disregarding frontal asymmetry to first order) provided an opportunity to examine the behavior of the gust front as a function of time and distance from its source. The met stations considered for this case, denoted in Figure 3c as numbered circles, are (1) Swiehan, (2) Alsad, (3) SMART (yellow circle), (4) Al Raknah, (5) Alhiyar, (6) Alfoah, and (7) Khatam Al Shaklah.

[40] Distances between these stations and the approximated origination point of the downburst were computed along with time-differences between the radar-inferred haboob arrival and the time of peak surface winds speed recorded at each station. The peak wind speeds were adjusted by adding/subtracting the vector component of the previous hour time-averaged environmental flow in the direction of the haboob. The data, shown in Figure 4, indicate an exponential decay in the peak wind speed ($U_{\max}$) with increasing radius, and an apparent increase in time delay (T_{dly}) between the first arrival of dust and that of the peak winds. This decay is explained primarily by mass continuity, wherein the wind speed is inversely proportional to radius from a steady, symmetric source. A secondary component is attributed to atmospheric and surface frictional dissipation forces acting on the outflow as it moves away from the localized forcing region (downburst), suggesting an eventual decoupling of the dust wall from the main cold pool air mass (characterized by meteorological parameter discontinuities at the front) similar to the observations of *Chen and Fryrear* [2002]. Although the structure of the haboob was not symmetric and was complicated by contributions from multiple convective cells, simple exponential curve-fits made to these station data (also shown in Figure 4) provide a first-order depiction of U_{max} and T_{dly} evolutionary behavior for this case:

$$U_{\max} = 27.3\exp(-0.069R) + 7.0 \tag{5}$$

and

$$T_{dly} = 1.1\exp(0.058R) + 9.4, \tag{6}$$

where R (the radial distance from the downdraft center to the gust front, assuming a symmetric outflow pattern) is specified in km. We take care to point out here that these coefficients are expected to change dramatically as a function of the ambient environmental conditions, and surface friction, and evolution of the convective forcing itself. Also, it is not clear whether the time delay between dust front and peak winds observed here is necessarily a characteristic of all haboobs, especially since the majority of previous reports do not give mention of such decoupling (albeit from point observations whose proximity to the downburst are unknown). The decoupling of dust from cold pool properties at great distances from the source may also be the result of frictional dissipation effects, where the "nose" dust lofted with the original downburst surge is no longer associated with strong winds or sharp gradients in T/P/Q, but is instead now being pushed along and mixed with the environmental air in advance of the main body of the cold pool.

[41] The 1-min time resolution SMART meteorological parameter observations are shown in Figure 5 along with the approximate period during which time the all-sky camera sensed high dust concentrations passing overhead (here, the "W" represents the direction of dust motion toward the west, away from the Al Hajar range). The data reveal only a minor pressure spike of ~0.2 mb, accompanied by a ~3.3 K temperature fall and 9% drop in relative humidity indicative of a dry microburst. Since wind speeds were not recorded at SMART, we invoked a relationship between peak wind gust and peak temperature departures between the environment and the cold pool, offered by *Proctor* [1988],

$$U_{\max} = -5\Delta T, \tag{7}$$

valid for peak temperature departures (ΔT) between 0 and −8 K. The estimated peak wind speed by this parameterization is 16.5 m s^{-1}.

[42] The MPL detected the cloud base height of the parent system at 5 km above ground level (AGL), and placed the

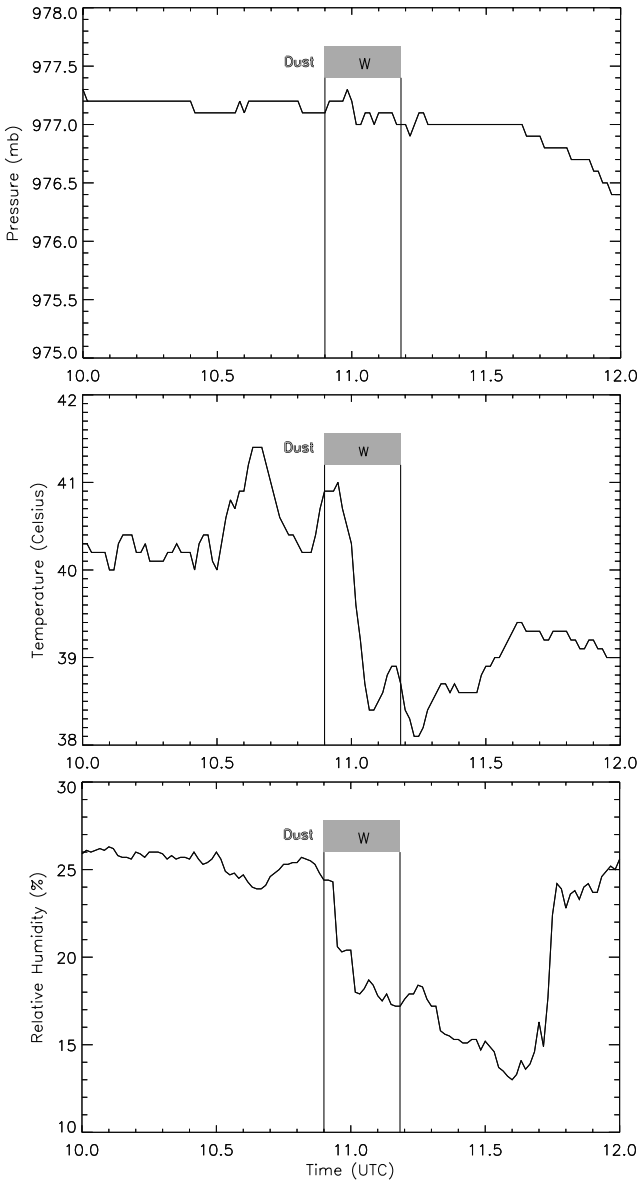

Figure 5. SMART station observations of (top) pressure, (middle) temperature, and (bottom) relative humidity for the 3 September 2004 haboob case. The time period when dust was observed by the station's all-sky camera is shown as a light gray box, and the "W" denotes the westward direction of dust motion.

haboob's height at 0.5 km AGL (see Figure 3b). Using the closest available sounding data (Abu Dhabi, 1100 UTC), cloud base pressure was estimated at 555 mb (near the base of a mid-level capping inversion). Calculations based on the cold pool temperature and dew point depression observed at SMART suggested that the virga shaft extended down from cloud base to 700 mb, below which point the parcel descent transitioned from a moist to dry adiabatic lapse rate. Combining this information with the virtual temperature profiles between cloud base and the surface for the environment and the cold pool parcel [e.g., *Wakimoto*, 1985, Figure 10], and assuming a downdraft wind speed of zero at cloud base, the downdraft wind speed at the surface (equation (2)) was computed as 20.3 m s^{-1}, of similar magnitude to the estimate based on *Proctor* [1988]. As an additional comparison, if the general observation of *Lawson* [1971] (being that the speed of dust advance is approximately half the maximum wind speed measured behind the front) holds true, then the Al Ain radar-inferred haboob speed (10.5 m s^{-1}) would then correspond to a maximum wind speed of 21 m s^{-1}. While the equation (2) result is also similar to the peak horizontal winds observed at the two met-stations closest to the haboob source (see Figure 4), we take care to point out that it may in fact underestimate the true peak winds produced by the downdraft due to the aforementioned 15 min averaging imposed on the met-station anemometer readings. Done as a preprocessing step at the automated station prior to reporting, this averaging would tend to bias the wind speed values low, especially if the true peak wind occurred over a duration that was significantly shorter than the averaging window.

4.2. The 13 September 2004 Nocturnal Case: Western UAE

[43] Unlike the majority of haboobs encountered during UAE^2, where the origins of multiple mid-day/late-afternoon convective cells were traceable back almost always to some point along the Al Hajar range, the mesoscale convective system that formed during the late-afternoon/early-evening hours of 13 September 2004 originated on the south-central border between the UAE and Saudi Arabia as a completely isolated event. Far removed from the SMART facility, and being primarily a nocturnal system, this convective complex was monitored primarily by satellites and a collection of coastal and offshore met-stations along the eastern UAE domain. The cloud system produced one of the largest haboobs observed during this study period, and the only one offering a mostly unobstructed view of the actual dust wall from the perspective of the higher spatial/spectral resolution LEO satellite observing systems.

[44] A suite of satellite observations depicting the evolution of this complex is shown in Figure 6. The UAE^2 met-stations located in the path of this system, indicated as numbered circles in Figure 6a, are as follows: (1) Al Qlaa, (2) (Algheweifat, (3) Sir Baniyas, (4) Dalma, (5) Makassib, and (6) Quarnen. In Figure 6a, the DMSP Operational Linescan System (OLS) nighttime visible band has been combined with its infrared band to reveal both lights (yellow) and cold cloud tops in blue, and Figure 6b shows the retrieved cloud top heights for the system based on the Meteosat-5/NOGAPS method mentioned previously. The DMSP/OLS enhancement is a bi-spectral (nighttime visible and 11.0 μm thermal infrared) technique described by *Miller et al.* [2005]. The white streak atop the blue cloud region in Figure 6a corresponds to a lightning flash captured as the OLS detector crossed atop the cloud (i.e., multiple return strokes causes the cloud to "flicker" for a fraction of a second, such that a linear segment of light is inferred by the rapidly scanning sensor detector element).

[45] In Figures 6c (Terra MODIS) and 6d (NOAA-17 AVHRR), a false color enhancement based on the nocturnal 11.0–3.7 μm brightness temperature difference sensitivity to certain mineral dusts [e.g., *Ackerman*, 1989] reveals the gust front as a thin red line propagating outward along an approximately 180° arc on the northern portion of the cloud

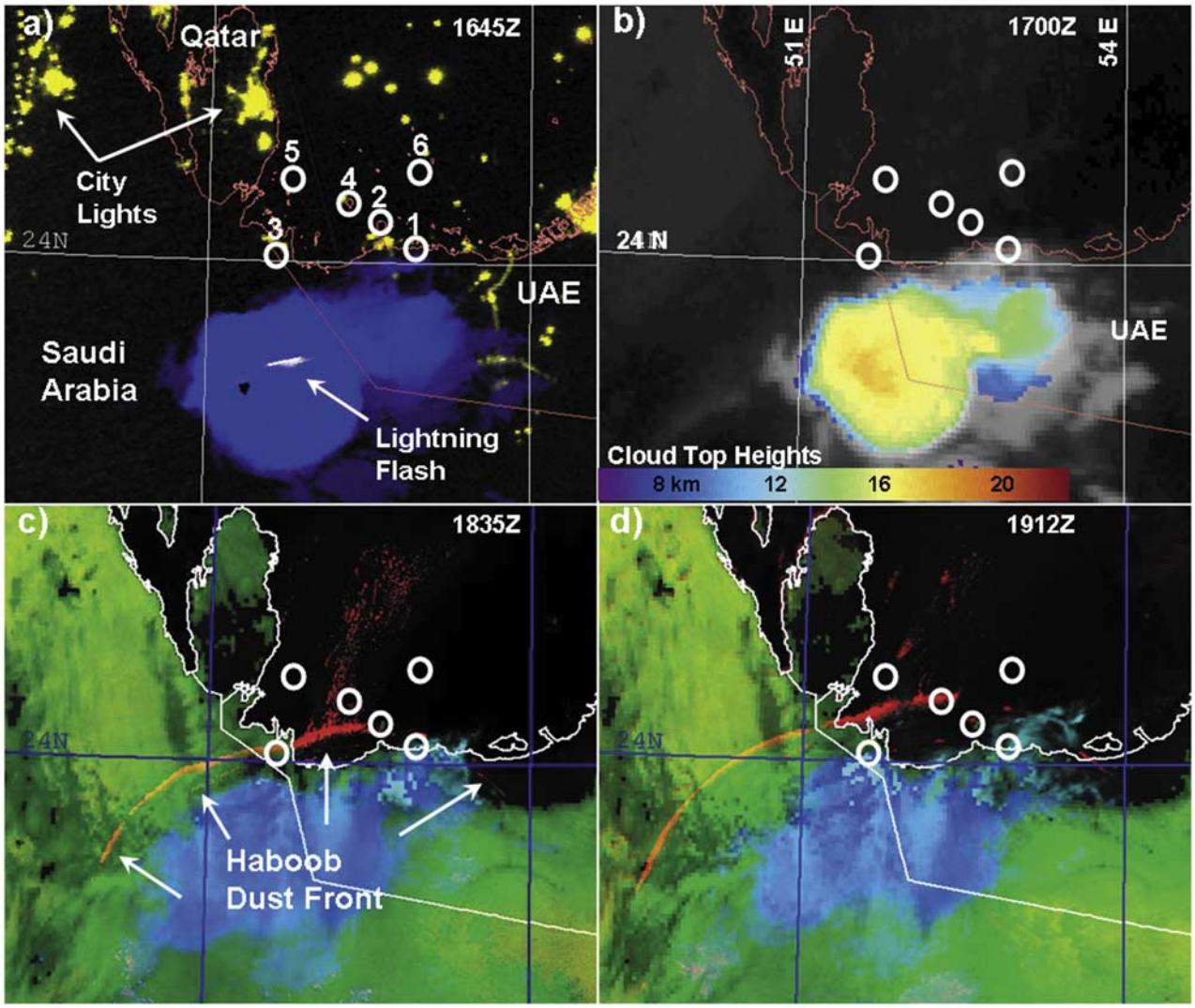

Figure 6. Multisensor co-registered view of a convective complex over the western UAE domain on the night of 13 September 2004: (a) DMSP/OLS nighttime visible showing the electrically active storm, (b) Meteosat-5 convective cloud heights showing significant cloud top heights (~18 km), (c) Terra MODIS dust enhancement (the possible haboob appears here as a red linear feature), and (d) subsequent NOAA-17 AVHRR dust enhancement showing frontal advance roughly one-half hour later. In Figures 6c and 6d, discrete patches of red off the eastern shore of Qatar are low-level cloud structures, also enhanced via this approach, and green areas correspond to false-positive land surfaces filtered out of the enhancement as a preprocessing step. See text for listing of meteorological stations, identified here as numbered circles.

complex. The enhancement is based on the 11.0 and 3.7 μm brightness temperature difference (here, enhanced scattering by mineral dusts in the near infrared can produce a positive value), encoded into the red channel of a conventional three-color composite [e.g., *d'Entremont and Thomason*, 1987], and 11.0 μm brightness temperature is encoded in the blue and green planes. In this way, the lower/warmer dust produces a bright red tonality and high/thick clouds become shades of cyan. This simple bi-spectral approach will not detect all nocturnal dust events, particularly optically thin plumes. The rapid cool-off at night of land skin temperature, and onset of low level temperature inversions, complicate the problem further.

[46] Important to note in Figure 6 is that scattering by small liquid droplets in low-level clouds also produces a strong 11.0–3.7 μm brightness temperature difference [e.g., *Lee et al.*, 1997], and in fact some clouds are evident offshore in Figures 6c and 6d. However, as seen here (and also in Figure 1), the haboob front produces a highly organized spatial structure with sharply defined outflow boundary that typically is readily distinguished from discrete/scattered cloud fields. Without radar, MPL, all-sky camera, or aerosol particle probe information for this remote case, we cannot provide irrefutable evidence that the structure identified as a haboob is not in fact arcus cloud (also known as "roll" or "shelf" clouds) forming along the

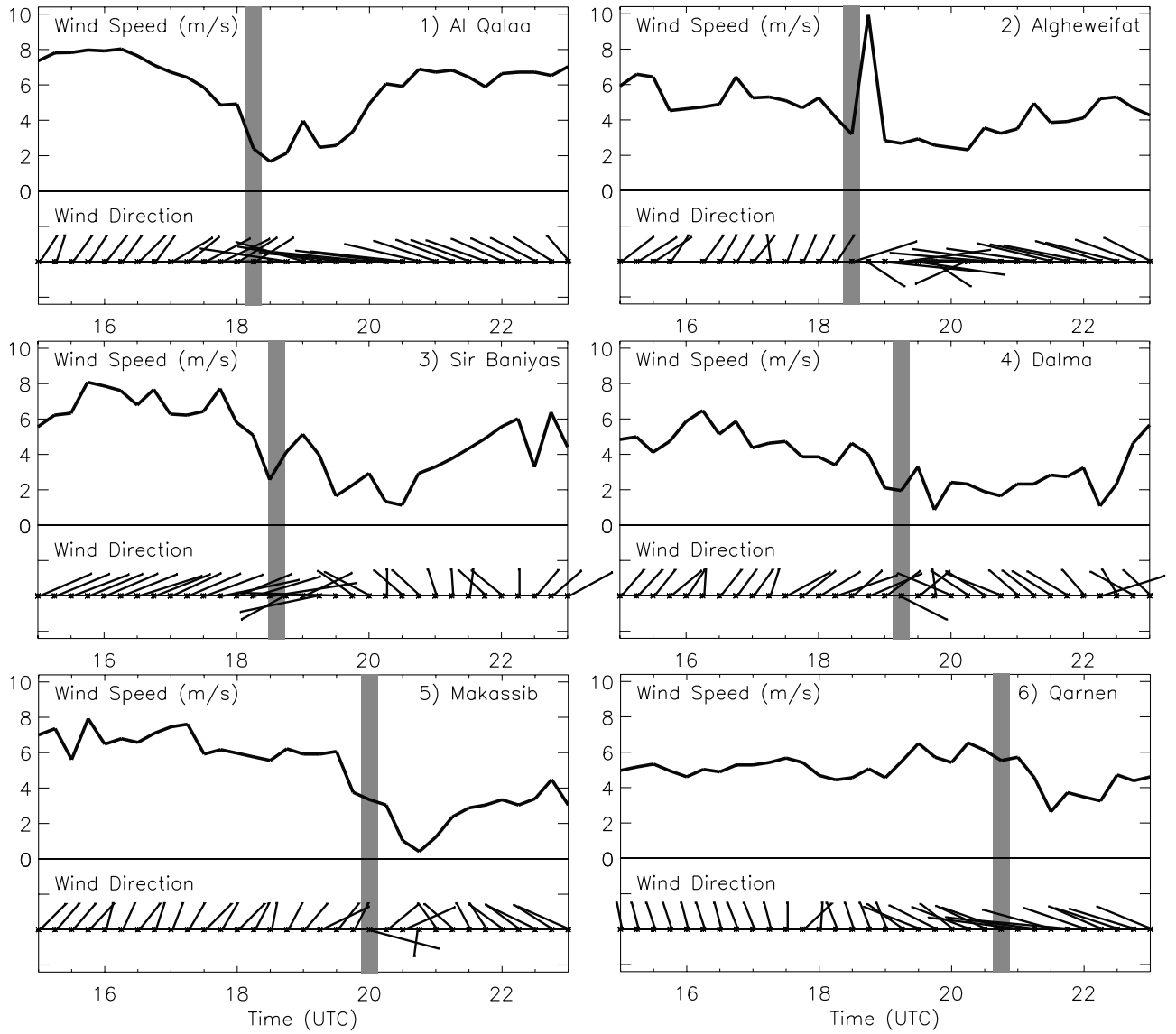

Figure 7. Wind observations from meteorological stations numbered as in Figure 6a for the 13 September 2004 case. Vertical gray bars denote the predicted haboob crossing times based on radial extrapolation of gust front speeds analyzed from the satellite imagery shown in Figures 6c and 6d.

gust front boundary [*Knippertz et al.*, 2007]. Close inspection of the northwestern quadrant of the outflow reveals an additional enhanced linear structure a few tens of km behind the main front, suggesting a secondary downburst from within the complex, as was also observed during the 3 September event.

[47] Since there was no radar data available at the time of this event for the purpose of timing the dust front crossing over the station network, we instead appealed to the two satellite dust imagery enhancements shown in Figures 6c and 6d. Fortuitously, the two overpass times corresponded very closely to when the haboob crossed over the Algheweifat, Sir Baniyas, and Dalma met-stations. For the remaining stations, the time of arrival was estimated by computing differences between the satellite-observed frontal positions along radial trajectories (i.e., normal to frontal propagation) toward the station in question. The rate of forward propagation based on this imagery analysis was far from uniform, due in large part to superposition of the parent system's north/northeastward motion. Frontal advance was estimated as 18 m s^{-1} near Sir Baniyas (within 15° of the parent storm motion vector) but only about 11 m s^{-1} near Al Qlaa (45°–55° clockwise from storm motion vector).

[48] Figure 7 shows time histories of the met-station recorded wind speeds and directions around the time of the haboob crossing. The stations are numbered as marked in Figure 6, in roughly sequential order with respect to the times of the haboob crossing. The satellite-estimated frontal passages (i.e., using the time-differencing method described above) are overplotted as vertical gray bands on each panel. Close inspection of the wind direction data reveals wind shifts and/or speed discontinuities in close proximity to the estimated frontal passages. The prevailing environmental winds were northerly (onshore and opposing the direction of the haboob, as previously noted by *Lawson* [1971]) during the period, such that combined with the 15 min time

averages produce either depressions in the wind speed and various degrees of rotation in wind direction, depending on the strength and longevity of the gust front. The only station to produce a strong spike in wind speed in the direction of the gust front outflow was Alghweifat, closest to the haboob origination, not surprising if one assumes an exponential decay of peak wind values as suggested by the 3 September case observations (Figure 4). On the basis of the coarse temporal resolution satellite imagery and time-averaged met-station data alone, there is insufficient data to determine conclusively any time delay between the haboob feature and the ground station wind-shift. However, the wind speed depressions and sustained deformation of the prevailing northerlies at both the Makassib and Qarnen stations farthest removed from the parent system do suggest a ~60 min delay in this peak from the estimated haboob arrival time.

4.3. The 22 September Case: SMART Station

[49] We include as a final case study one of the most visually impressive and well documented events observed during UAE^2. On 22 September 2004 at ~0900 UTC, a small cluster of convection developed over the Al Hajar Mountains just east of Alfoah and proceeded along a westward track. By 0940 UTC the Al Ain radar began picking up the first radially expanding signature of a downburst/haboob. While the main radar reflectivity core of the storm grazed the northern portions of Al Ain, the convective structure was highly variable and included at least one back-building stage (i.e., new convection forming to the immediate rear of the main cell motion). A summary of satellite, MPL, radar, and all-sky camera observations centered about the time of the haboob crossing at SMART are shown in Figure 8. The MPL data shows a dust layer depth of only ~300 m and cloud base height of ~3.5 km. Hand analysis of the 1100 UTC Abu Dhabi rawinsonde data produced a CCL estimate of 3.3 km.

[50] The SMART station all-sky camera first noted the approach of anvil cirrus accompanied by a darkening eastern horizon at 1000 UTC, followed by the abrupt arrival of a powerful haboob from the northeast at 1030 UTC. The initial dust wave cleared by 1037 UTC, giving way to light rainfall (visible as droplets on the fish-eye mirror). Intermittently between 1115-1145 UTC a series of smaller dust waves, this time traveling in the reverse direction (i.e., from west to east), crossed over the station. Time series of satellite imagery confirm that these secondary or "back-side" dust surges, the most pronounced of which occurred near 1145 UTC, must have originated from the same storms that produced the initial westward-traveling haboob. To the north and west of SMART at later times, the radar data indicated a complicated superposition of multiple gust fronts heading westward. In some cases a cell would regenerate, sending new outflows that overtook the previous ones (such a process could have been responsible for the secondary haboob mentioned in the previous 13 September case). The radar also suggested convective clouds being enhanced where gust fronts converged, including a collision with the northerly sea breeze front near 1300 UTC.

[51] The corresponding time series of SMART station observations for pressure, temperature, and relative humidity are displayed in Figure 9. As in Figure 5, the "W" corresponds to dust fronts propagating westward, while "E" denotes eastward-propagating dust fronts (i.e., back toward the Al Hajar range). A distinct pressure spike and simultaneous drops in temperature and relative humidity at the moment of the all-sky camera and Al Ain radar observed dust arrival indicates that the haboob dust resided entirely within the initial gust front. Immediately following the frontal passage, mesoscale high pressure developed as the main body of the evaporative cold pool advanced over the station and was accompanied by a ~25 min period of light rain, an additional temperature drop, and increased relative humidity. As the convection continued to move east the air temperature began to rise, when suddenly at 1117 UTC an apparent secondary downburst pulse sent a smaller back-side haboob (i.e., traveling eastward, and opposite to parent storm motion) across the station. In contrast to the initial haboob passage, the back-side haboob was accompanied by only a minor pressure jump but had comparable temperature and relative humidity to the recently passed cold pool. Back-building of the storm immediately to the east of SMART resulted in more light rain and additional eastward tracking haboobs at 1130 and 1142 UTC, with durations of these events as indicated in Figure 9.

[52] Although some light rainfall was observed with this system, the case still falls under the category of a dry microburst given the environmental conditions and observed behavior of the temperature/relative humidity fields. *Caracena et al.* [1983] note characteristic atmospheric profile structures associated with dry microburst days during the JAWS field experiment. The structure consists of a deep, dry sub-cloud layer and a moist layer aloft with cloud bases residing at mid-levels (~500 mb). As a metric for identifying environments favorable for supporting dry microbursts, the authors propose a "dry/wet" condition (DW) flag, defined as a comparison between the dew point temperature depressions near 500 mb and 700 mb:

$$\text{If } \left[(T - T_d)_{500\text{mb}} < 8^\circ C\right] \text{ and } \left[(T - T_d)_{700\text{mb}} > 8^\circ C\right], \quad \text{then } DW = 1. \tag{8}$$

[53] On the basis of the Abu Dhabi 1100 UTC sounding for the 22 September 2004 case, the dew point depressions at 528 mb and 700 mb were 4 °C and 17 °C, respectively, readily triggering this DW flag.

[54] Following the same procedure as in the 3 September case, we applied equation (2) to the Abu Dhabi 1100 UTC sounding and used SMART-measured cold pool temperature and dew point information to compute a downburst wind speed of 33 m s^{-1}. This is of similar magnitude to the peak wind estimated from equation (7) (38 m s^{-1}, based on a 7.6 °C temperature drop). *Brown et al.* [1982] demonstrated a novel application of Bernoulli's equation to the estimation of wind speed at the moment of gust frontal passage. Under simplifying assumptions of the frictionless, steady flow of a constant density fluid, the frontal wind speed can be thereby expressed as a function of the pressure change measured during and immediately following passage of the gust front:

$$v = \sqrt{(2\Delta p/\rho_{air})}, \tag{9}$$

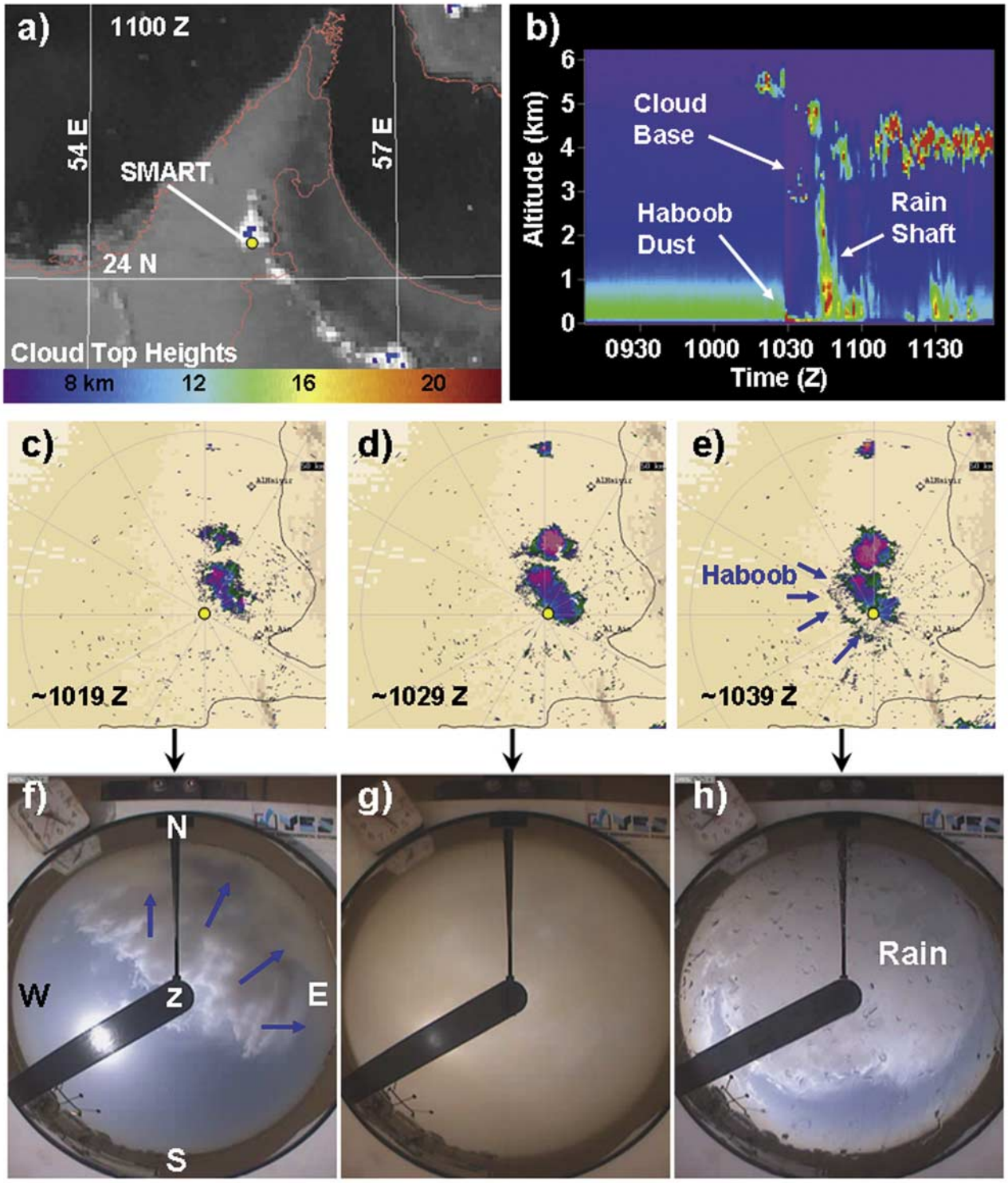

Figure 8. The 22 September 2004 haboob case as observed at Al Ain by (a) Meteosat-5, (b) the NASA MPL, (c-e) the C-band radar (yellow dot denotes Al Ain/SMART; blue arrows identify haboob outflow), and (f-h) the SMART all-sky camera (N/S/E/W denote approximate compass bearings, "z" denotes local zenith, and blue arrows show approaching/receding dust) as the dust front passed over the station. MPL imagery courtesy of NASA, and radar imagery courtesy of the UAE/DAS.

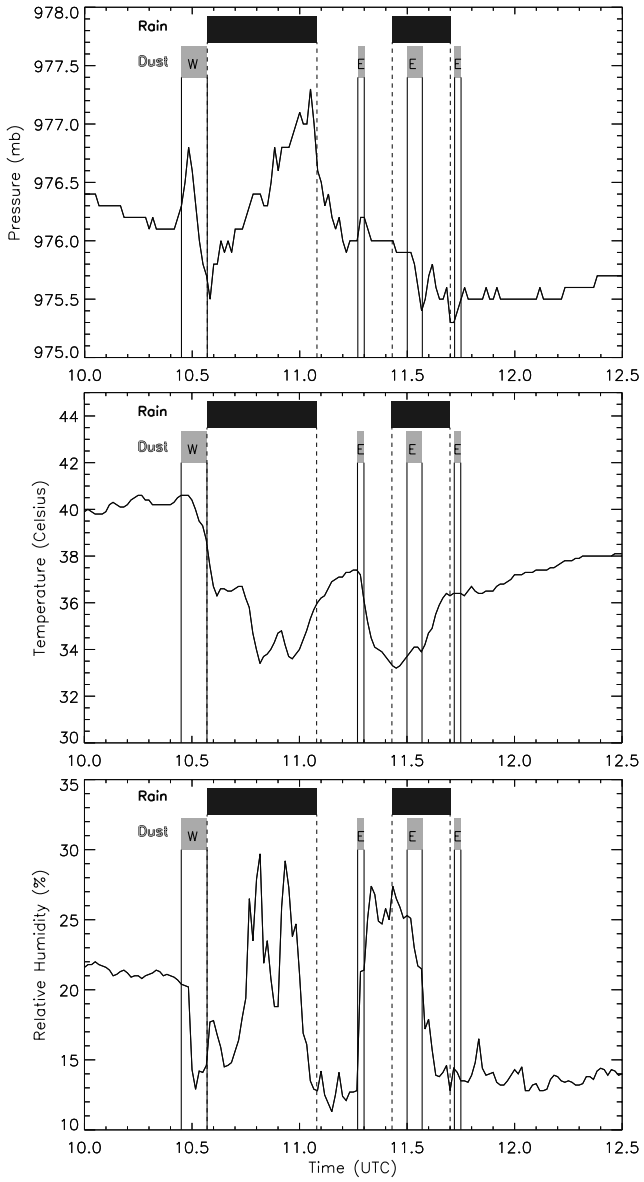

Figure 9. SMART station observations of (top) pressure, (middle) temperature, and (bottom) relative humidity for the 22 September 2004 haboob case. The time periods when dust was observed by the station's all-sky camera are shown in light gray boxes (with "W" and "E" denoting either westward or eastward direction of dust travel, respectively), and rainfall periods are shown as black boxes.

where ρ_{air} is the air density near the surface. Using measurements from SMART, which recorded a 1.3 mb pressure change for the 22 September 2004 haboob event, equation (9) produces a frontal wind speed estimate of 15 m s^{-1}. At first this may appear to be a substantial underestimation to the ~30 m s^{-1} estimates computed above. However, we recall that the Bernoulli wind speed estimate corresponds not to the peak wind, found *behind* the front, but to the velocity of the gust front itself. On the basis of differential analysis of the Al Ain radar imagery, frontal motion was approximately 14 m s^{-1}, in close agreement with this Bernoulli estimate. This value is also consistent with previous observations by *Lawson* [1971] of roughly a factor of two difference between frontal wind speeds and peak wind speeds associated with the cold pool. As such, there appears to be consistency among several independent methods for determining the haboob wind properties for this particular case.

[55] In spite of a very dry lower atmosphere (the Abu Dhabi sounding for this day shows a dry adiabatic lapse rate with relative humidity between 15–40% in the lower 5 km of the troposphere), the small amount of surviving rainfall observed at the surface suggests a high production of rainwater by this cloud system. We recall from section 2.1 that this condition favors the formation of stronger downbursts. However, it should also be pointed out that the MPL-observed cloud base for this case was slightly lower (by ~1 km) than in the 3 September case, increasing the odds of precipitation reaching the ground prior to evaporation. Given that the significant haboob of 22 September was produced by what certainly did not appear as a strong storm from the satellite perspective (having a relatively low cloud top height and being short-lived, e.g., in comparison to the previous two cases), we must conclude that satellite imagery of cloudiness alone is not a reliable indicator of where notable events are likely to occur. This message is reminiscent of the one delivered by *Wakimoto* [1983] in the context of an surprise tornado spawned in the Midwestern United States whose parent convective system did not produce the hallmark satellite indicators of a severe storm.

5. Ensemble Analysis

[56] To gain further insight and complement the case study analyses presented above, the UAE^2 haboob data were also examined in a statistical context. Conducting a day-by-day analysis of archived satellite imagery from Meteosat-5 for the UAE^2 study period bounded by 30 July to 30 September 2004 (62 days total), we determined that slightly more than half of the days (36, or 58%) produced significant convection (defined here as those cells whose maximum observed cloud top heights exceeded 6 km) along the Al Hajar range. The data, representing a total of 119 significant convective cells tallied over the two month period, are shown in Figure 10. The significant convection typically was observed to occur as clusters of adjacent days, separated by 3–7 day periods of no activity. During the Southwest Monsoon season (June to September) a quasi-permanent upper air ridge forms over the Arabian Peninsula and Iran. Surface-based and mid-level convection generally is suppressed by the warm, subsiding air associated with this high pressure system. However, deformation and/or shifting of the ridge structure in response to the passage of migratory weather systems allows for episodic moisture intrusions and increased instability, supporting the periods of enhanced regional convective activity seen in Figure 10.

[57] The clusters of convectively active days increased in duration over the study period from 2–4 days in early August, to 7–9 days by late August, to 16 days in late September. For a given cluster, the total number of significant convective cells produced reached a peak toward the middle of the period and tapered off on either side. There was also a notable increase in the peak number of signif-

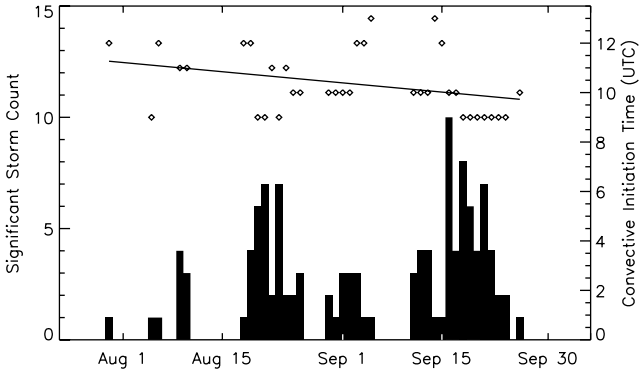

Figure 10. Time series of significant convective cells observed by Meteosat-5 along the Al Hajar mountain range during the UAE^2 field program (bars), and approximate convective initiation times (diamonds) with linear fit (line) to show trend.

icant cells within a given cluster over the course of the study period (ranging from 4 in early August, to 7 in late August, and 10 in late September). Convective initiation times, determined to within 30 min uncertainty, ranged from 0900-1300 UTC (1300-1700 local time), with a slight trend toward earlier initiation times over the course of the study period (as suggested by the linear fit made to the data shown in Figure 10). We detected no obvious correlations between the cluster structures and the physical location of convective initiation along the Al Hajar range. The above analysis was complicated on several convectively active days by limitations in the spatial (4 km) and temporal (30 min) resolution of the Meteosat-5 data in the presence of numerous cells following complex patterns of evolution (as suggested by the high resolution Al Ain observations noted in case studies above).

[58] On the basis of this ensemble data set, we set out to examine the time-dependent behavior of wind speed, temperature, pressure, and relative humidity of the gust fronts. From the 36 potential case days mentioned above we selected a subset of 7 days for intensive study. Using the UAE^2 met-station network, a combined 78 frontal passages from approximately 32 convective cloud systems were recorded. Many of the meteorological parameters in these cases demonstrated complex temporal behavior due to multiple gust fronts from surrounding storms, storm motion superposition, or the presence of other environmental factors such as the SBF. Cases under the obvious influence of these factors were flagged and removed using a combination of the Navy's Coupled Ocean-Atmosphere Mesoscale Prediction System (COAMPS^{TM}) [see *Hodur*, 1997] surface wind analyses, satellite imagery, and radar data whenever available. Finally, a subset of 10 idealized frontal passages that featured primarily isolated, clearly defined gust front passages with minimal complicating features was used for the ensuing analysis. It should be pointed out that since the SMART station provided the only visual confirmation of dust, a subset of the ensemble data set are not in fact confirmed haboobs. However, the assumption of dust production is deemed reasonable here in light of the characteristically high erodibility factors and low threshold friction velocities of the region, the low probability of significant soil moistening, and the high wind speeds observed for the events in question.

[59] The ensemble case results, centered about the peak wind recorded during the 10 idealized frontal passage, are shown in Figure 11. Pre-haboob environmental values for each case were removed prior to computing the ensemble, such that each curve represents departure from a basic state. Mean wind speed peaked near 10 m s^{-1}, surface pressure rose by 2 mb, air temperature dropped by 7 °C, and relative humidity increased by 15%. It should be noted that these results have not been stratified according to proximity of the station to the haboob source, such that space-time dependencies (e.g., wind speed magnitude vs. radial distance) are not captured. Also, we reiterate the important point concerning parameter smoothing for these 15 min averaged data. All extrema in Figure 11 were found to coincide with the peak wind time with the exception of surface pressure, which exhibited an approximately 30–60 min lag. In addition, all parameters began to change prior to the peak wind time (indicating potentially large separation between the front and main cold pool properties) and then settle toward pre-storm levels after peak time. Variance in the surface pressure, air temperature, and relative humidity were large, particularly after peak wind time, pointing to the inherently large variability of the cold pool properties. In particular, relative humidity was often observed to either increase or decrease dramatically with time (e.g., Figure 9) for a given event.

[60] Considering the basic environmental state itself, Figure 12 shows the Abu Dhabi nighttime (2300 UTC) and daytime (1100 UTC) soundings of temperature and dew point temperature (means and standard deviations) for the same subset of case-days used for Figure 11. Striking features include (1) the extremely dry lower troposphere accompanied by steep temperature lapse rates, (2) a layer of mid-level moisture between 500–600 mb, and (3) rapid drying above 500 mb. During the day, the average lapse rate between 1000 and 650 mb was 8.3 K/km (max −9.2 K/km), and was often accompanied by a shallow super-adiabatic layer adjacent to the hot skin temperature of the surface. At night, this lowest layer was replaced by a relatively moist inversion. There are marked similarities between Figure 12 of this paper and Figure 8 of *Wakimoto* [1985] corresponding to dry microburst days on the high plains of Colorado.

[61] Finally, calculated mean profiles of daytime relative humidity and equivalent potential temperature (θ_e, calculated via the method of *Bolton* [1980]) for the same case-day ensemble are shown in Figure 13. Similar to the DW flag, *Atkins and Wakimoto* [1991] use the θ_e profile as a stability index for predicting microburst potential. Here, a difference between the surface θ_e and its minimum value aloft is computed, with microburst days correlating positively with differences of 20 K or greater and null days dominating the statistics whenever the difference falls below 13 K. The metric was developed originally in the context of assessing wet microburst potential, but speaks in this case to the general atmospheric preconditioning which supported haboob production. The calculation based on the mean θ_e profile of Figure 13 (using values computed for the surface and 550 mb) was 30 K, suggesting that the appropriate

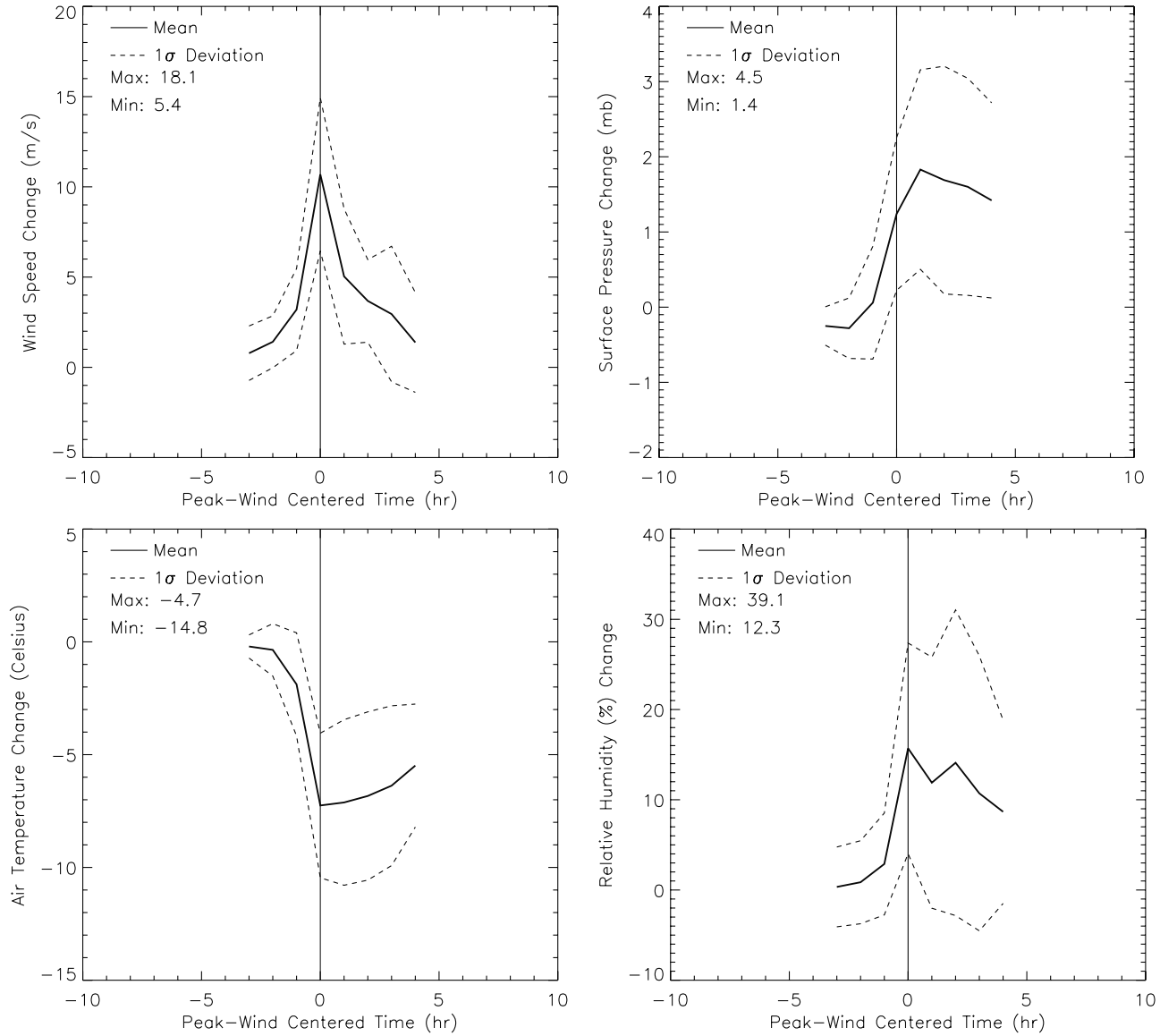

Figure 11. Means (bold/solid curves) bracketed by one standard deviation (light/dashed) for wind speed, pressure, temperature, and relative humidity based on the 10 ideal-case haboob frontal passages described in section 5. Data are centered about the time of peak recorded wind speed.

instability and moisture conditions were in place on these haboob-producing days.

6. Regional Aerosol Budget Impacts

[62] The high number of potential events shown in Figure 10 suggests that the contribution of haboob dust to the regional background aerosol loading during the summer months may be significant. To quantify this statement, we developed a highly idealized numerical model of dust production by downburst forcing occurring over a finite area and for a finite duration. We assumed for simplicity an axisymmetric, radially propagating cold pool outflow pattern produced by a dry microburst (i.e., no soil moistening from rainfall) expanding across a homogeneous erodible desert surface. Implicit to our assumptions of symmetry are that there is no environmental flow, storm motion, or processes resulting in the transport mid/upper-tropospheric horizontal momentum down to lower-levels. In light of the UAE topography and generally weak flow observed both at the surface and aloft during the study period, we claim that these simplifying assumptions preserve the integrity of a first-order approximation.

6.1. Model Theory

[63] There are several other physical constructs and associated model parameters which must be specified in this model, foremost among them being the surface wind speed and its assumed space/time variation. First, we recall from Figure 4 the approximate exponential decay of the observed peak wind speed with radial distance from the point of initial downburst impact with the surface. To parameterize this behavior in our model, we assumed a characteristic initial value of wind speed at the downburst

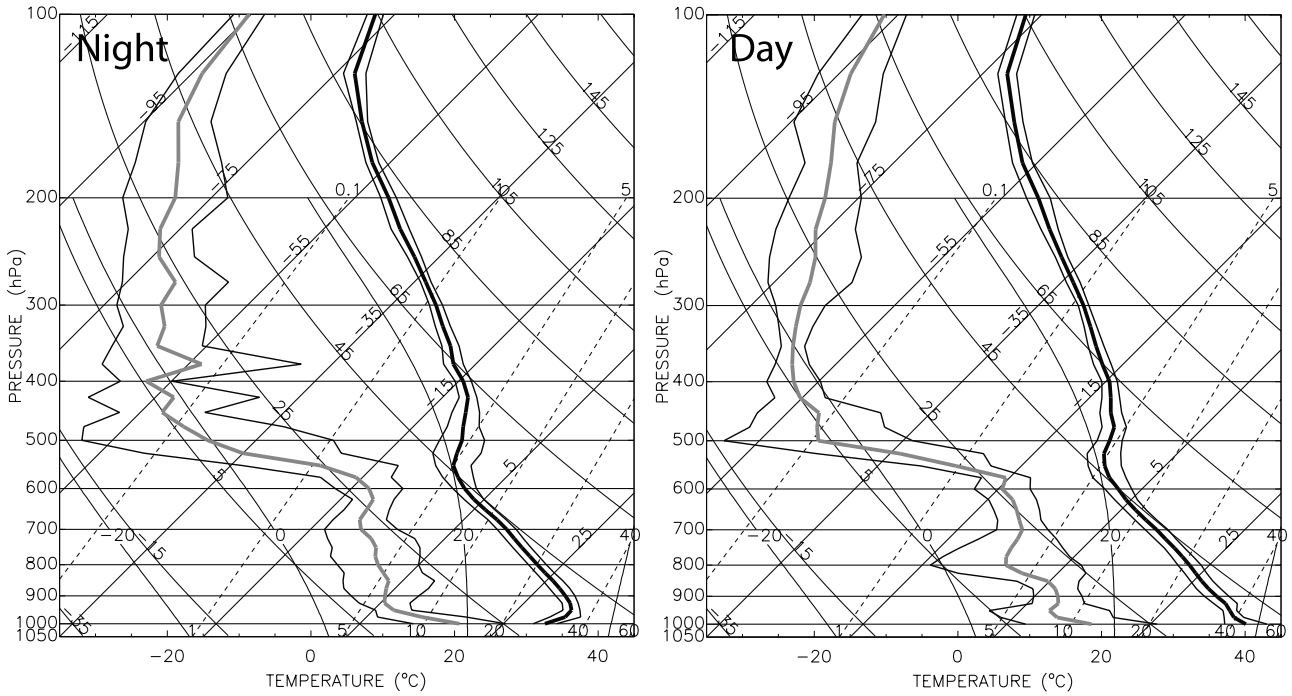

Figure 12. Abu Dhabi rawinsonde mean nighttime (2300 UTC; 0300 local) and daytime (1100 UTC; 1500 local) data plotted on Skew-T/Log-P diagrams based on the 7-day subset of ideal haboob cases considered in section 5. Mean dew point temperatures are shown in light gray, and temperature profile is shown in black, bracketed by one standard deviation.

origin (e.g., 30 m s^{-1}, based on extrapolation of Figure 4) and applied an exponential decay factor to represent the radial-variation of its initial magnitude. We also needed to specify the temporal behavior of the wind speed at a fixed location following the arrival of the gust front. On the basis of time series of wind observations from UAE met-stations closest to downburst origination points, we found that usually the gust front arrives coincident with the peak wind speed and decays exponentially thereafter. This is a simplification to the actual wind speed structure, but it remains consistent with the general behavior observed in close proximity to the source where deflation processes presumably are at their strongest.

[64] The total mass of dust lifted by this idealized system is estimated by

$$M_d = \int_{\theta=0}^{2\pi} \int_{r=0}^{R_c} \int_{t=0}^{t_c(r)} F(t,r,\theta)\, dt\, r dr\, d\theta, \qquad (10)$$

where $F(t, r, \theta)$ is the dust source flux from the land surface, parameterized by equation (4). On the basis of station observations of haboob passages and the peak-wind decay structure noted in Figure 4 and discussed above, we assumed here a space/time-variable friction wind velocity of the form

$$u_*(r,t) = U_0^* \exp(-s_1 r) \exp(-s_2 t), \qquad (11)$$

where s_1 and s_2 are coefficients of wind speed decay as a function of radius (r) from the downburst impact with the surface and time (t). The spatial decay coefficient for initial wind speed at the origin of the downburst (s_1, having units of inverse distance), which physically is a function of mass conservation and atmospheric/surface dissipation terms (friction) as mentioned previously, is assumed here to be

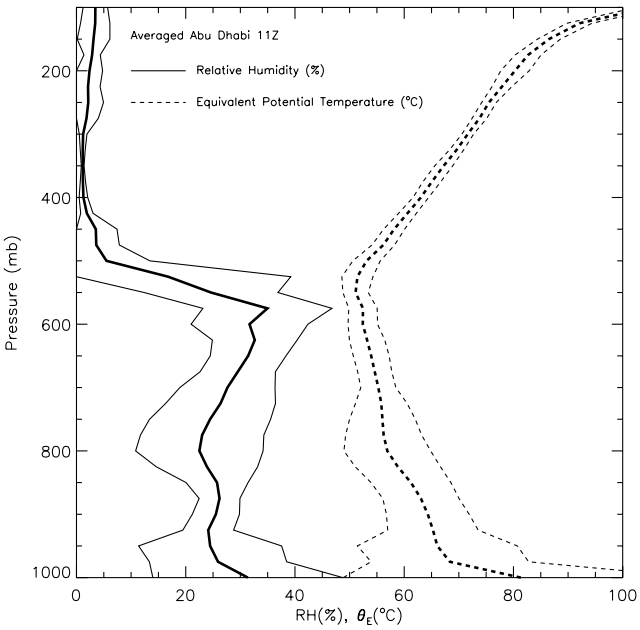

Figure 13. Abu Dhabi rawinsonde-derived mean daytime (1100 UTC; 1500 local) profiles of relative humidity (solid) and equivalent potential temperature (dashed) based on the 7-day subset of ideal haboob cases considered in section 5. Bold curves denote means, and lighter bracketing curves denote one standard deviation.

symmetric about the origin and approximated by the exponential coefficient specified in equation (5) (i.e., 0.07). The time decay coefficient for post-frontal wind speeds at a given location (s_2, having units of inverse time) is parameterized as a function of both the initial friction velocity (U_0^*, defined at the downburst source), the threshold friction velocity (U_T^*), and the "effective duration" of the downdraft itself (T_{DD}; the duration over which the frictional velocity exceeds the threshold for deflation, U_T^*) measured at the downdraft source. Assuming that the temporal decay behavior is independent of radius (as it should be for a homogenous surface), we can set r = 0 in equation (11) and evaluate s_2 at $u_* = U_T^*$ and $t = T_{DD}$:

$$s_2 = -\frac{1}{T_{DD}} \ln\left(\frac{U_T^*}{U_o^*}\right). \tag{12}$$

[65] For a given peak wind speed, a short-lived downburst would correspond to a much steeper decay rate toward zero-dust-lifting than a long, sustained downdraft. The implicit assumption, supported by the observations of *Idso et al.* [1972], *Chen and Fryrear* [2002], and the current UAE^2 data set, is that the downdraft intensity is not constant (step function) at the source but instead falls off gradually from its peak value over time. In summary, as the gust front propagates away from the source the initial (peak) wind speed is reduced by conservation of mass and friction effects (with decay parameterized by s_1), and at a fixed location decays after frontal passage according to the downdraft structure itself (s_2).

[66] In specifying equation (10), the initial friction velocity (U_0^*) was computed using equation (3) with values representative of a desert surface in an unstable daytime environment (κ = 0.4, z_s = 10 m, z_o = 0.01 m, and $z/L = -2$) and a parameterization for the momentum stability parameter:

$$\psi_m = 2\ln\left(\frac{1+x}{2}\right) + \ln\left(\frac{1+x^2}{2}\right) - 2\tan^{-1}(x) + \frac{2}{\pi}, \tag{13}$$

where

$$x = (1 - 15(z_s/L))^{0.25}. \tag{14}$$

[67] The critical radius for deflation, R_c, defined as the radius at which the peak friction wind velocity (i.e., specified at t = 0; the gust front arrival) falls to the friction velocity threshold (i.e., U_T^* and $t = T = 0.6$ m s^{-1}, following *Gillette and Passi* [1988] and *Westphal et al.* [1988]), was obtained by solving equation (11) for r:

$$R_c = -\frac{1}{s_1} \ln\left(\frac{U_T^*}{U_0^*}\right). \tag{15}$$

[68] No new dust is lifted beyond R_c. For all radial distances $r < R_c$ there will be a critical time duration, t_c (defining the upper bound for the time integral in equation (10)) over which dust will be lifted, governed by the downdraft structure described in equation (12). This critical time was found by solving equation (11) for t evaluated at the point when the friction wind velocity decays to the friction velocity threshold (U_T^*):

$$t_c(r) = -\frac{1}{s_2}\left[\ln\left(\frac{U_T^*}{U_0^*}\right) + s_1 r\right]. \tag{16}$$

[69] Together, equations (15) and (16) define the spatial and temporal bounds of deflation by our modeled haboob. There is a log linear drop-off of the dust source flux with increasing radius and time owing to the decay assumptions imposed in equation (11), and integration of this production over space and time yields the total dust mass lifted for a given event.

[70] To recap, the governing parameters of this simplified haboob deflation model are the peak initial friction velocity (U_0^*), its radial dissipation rate (s_1), and the time decay of wind speed (s_2) expressed as a function of the downdraft duration (T_{DD}). The parameters are related explicitly to the strength of the downburst (a function of the environment and cloud properties) and implicitly to surface-environmental dissipation properties. Therefore any transport and dispersion model capable of simulating (at sufficient spatial resolution) mesoscale convective clouds and specifying the above parameters would in principle be equipped to include transportable dust contributions from haboobs. It is also important to note that we have assumed that dust is being lifted continually for as long as the space-time dependent friction wind exceeds the threshold velocity for deflation. This may not be the case in reality if the amount and/or distribution of available deflatable material changes with time, hence changing the source flux relationship itself (i.e., equation (4)).

6.2. Haboob Simulations

[71] The results for the model, displayed in terms of total dust production (kg) and the concentration (mass of dust per volume of air; μg/m^3) of dust available for long-range transport (i.e., fraction of the total deflated concentration), are shown in Figure 14. The radial dissipation rate (s_1) was assumed fixed as stated above, the threshold friction velocity was specified at 60 cm/s, the peak initial wind speed U_0(defined at $r = 0$ and related to the peak initial friction velocity U_0^* via equation (3)) and downdraft duration T_{DD} were the free variables. For typical values of downdraft duration (T_{DD}) and U_0 spanning perhaps 10–40 m/s, the model suggests a 2–3 order of magnitude overall variation in both total mass and transportable concentration. While such values of 1–10 kilotons of dust raised by a single haboob event may at first seem unrealistically large, the corresponding area-averaged "scouring depth" (assuming for simplicity a cylindrical volume characterized by the critical radius, R_c) is only about 1–5 μm when assuming a dust density of 2.5 g/cm^3 (e.g., J. S. Reid et al., An assessment of size distribution of airborne dust particles with implications for model applications, submitted to *Journal of Geophysical Research,* 2006). As expected, dust production was reduced for lower peak winds and shorter durations and maximized for the reverse. The sudden decline to zero production at wind speeds less than about 10 m s^{-1} was due to our imposed friction velocity threshold.

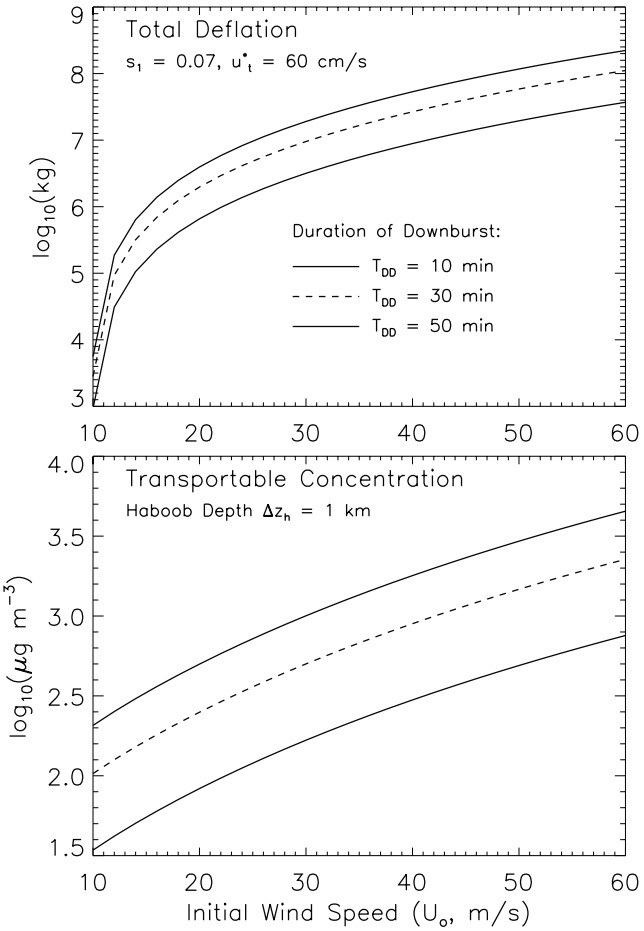

Figure 14. (top) Total lifted dust mass and (bottom) transportable dust concentration for an idealized haboob plotted against initial gust front wind speed (at downburst origin) for selected downdraft durations. Model parameter constraints include a threshold friction velocity of 60 cm/s, a radial decay factor of 0.07, and a dust layer confined to the lowest 1 km of the atmosphere.

[72] The transportable concentration (4.4% of total production, following *Westphal et al.* [1988]) was estimated by distributing the total deflated dust mass over the cylindrical volume of deflation, according to

$$C_T = \frac{0.044 M_d}{\pi R_c^2 \Delta z_h}, \tag{17}$$

using equations (10) and (15), and assuming a haboob thickness of Δz_h (taken here as 1 km). The events observed at Al Ain for the 3 September and 22 September case studies suggested thicknesses on the order of 0.5 km, such that the corresponding concentrations in Figure 14 would be doubled (i.e., adding a factor of ln(2), or roughly 0.7, to the log-scaled results shown in Figure 14). The magnitude of transportable dust concentration, ranging from about 1.0×10^2 to 2.0×10^4 μg/m^3, is consistent with the range of concentrations produced by the COAMPS^{TM} model for similar magnitudes of friction wind, albeit over extremely localized areas. Over the peak initial wind speed range of 10 m s^{-1} to 40 m s^{-1}, for example, the critical radius (R_c) varied nonlinearly between 0.6 and 26.2 km. This should not be misinterpreted as characterizing the maximum radial distance traversed by the haboob dust wall itself, but rather, the radial distance over which actual deflation occurs (i.e., dust is subsequently transported downstream). It is important to point out that in reality the fine-mode dust component is transported radially after its initial deflation, combining with newly lifted dust along the front to produce much higher transportable concentrations along the leading edge of the haboob. From the perspective of long-range transport or background aerosol loading, these local/transient distribution errors hold less significance.

[73] Using in situ observations, *Chen and Fryrear* [2002] report a peak concentration of 1.3×10^3 μg/m^3 (or, 3.1 in $\log_{10}$ units) for the Big Spring, Texas haboob, which happens to fall within the model solution space drawn in Figure 14. The comparison is again complicated by the fact that no dust-removal (e.g., sedimentation) processes or vertical structure are included in our simple model. *Chen and Fryrear* [2002] estimate a total horizontal mass flux of $\sim 8.5 \times 10^4$ kg/m^2-hr, based on a vertical integration (from the surface to $\sim$16 m above ground level) of total mass collected over the duration of the event. While the actual instantaneous horizontal flux (F_H) will be a strong function of both space and time, we can compute an equivalent total horizontal mass flux for our haboob model by combining the total concentration (equation (17), with the 4.4% fine-mode factor removed via normalization) with a characteristic velocity defined by the critical radius (equation (15)) and downdraft duration (T_{DD}):

$$F_H = \frac{C_T R_c}{0.044 T_{DD}}. \tag{18}$$

[74] As defined, this mass flux integrated over the entire duration of the haboob considers all material. It is therefore independent of the downdraft duration but varies with downdraft strength. Applying equation (18) to a range of initial gust front wind speeds (say, 12 to 34 m s^{-1}) produced horizontal fluxes ranging from 1.8×10^4 to 7.2×10^5 kg/m^2-hr. In particular, an initial peak wind speed of 18 m s^{-1} produced a modeled dust flux of 8.7×10^4 kg/m^2-hr, close to the *Chen and Fryrear* [2002] estimate for the Big Spring, Texas event. The requirement changes to 23 m s^{-1} if we assume that only half the material physically lifted was collected (e.g., due to sedimentation processes), and to an unrealistic 54 m s^{-1} if we assume only 4.4% of the total distribution was collected (i.e., considering only diameters <10 μm, but this assumption would in turn be inconsistent with the maximum particle sizes of 40 μm the authors observed for this event). Higher erodibilities, e.g., over freshly tilled Texas farmlands, could in turn bring down those wind speed requirements.

[75] While these proxy comparisons are encouraging, we are mindful of the fact that the concentration/flux agreement demonstrated between this simple haboob model, COAMPS^{TM}, and available observations is useful only as a first-order sanity check and is not intended to represent validation. There are many simplifying assumptions, parameterizations, and ancillary data requirements (particularly with respect to its necessary coupling to a representative

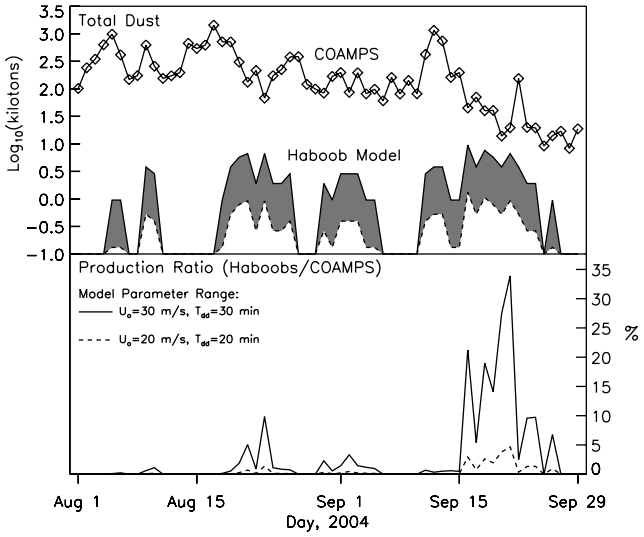

Figure 15. Comparison between COAMPS™ and haboob model of transportable dust mass lifted over a two month period for a 1000 × 1000 km area centered about the UAE study domain. Haboob production estimates were bracketed by two representative examples of initial wind and downburst duration applied to equations (10)–(16), using storm frequency reported in Figure 10. The top panel shows total dust production, and the bottom panel shows relative significance of haboob contributions over the region.

convective cloud dynamics and microphysical model, and as suggested above, space-time-dependent source and removal processes) precluding its direct implementation within an aerosol transport and dispersion model. Nonetheless, this physically based model does appear to perform at a level sufficient to apply it here to the estimation (within an order of magnitude) of fine-scale bulk dust production by haboobs.

6.3. Gauging Regional Influence

[76] To approximate the relative importance of haboobs to the total regional dust burden, we compared for a given time period the total transportable dust mass generated locally by haboobs to that lifted by other dynamic mechanisms over the broader, regional domain. The study domain, a 1000 × 1000 km box centered on (23.8 °N, 54.3 °E), was selected to capture significant regional-scale deflation events observed over the study period. We ran the COAMPS™-forced aerosol model to provide hourly domain-integrated estimates of dust production over the period 1 August to 29 September 2004, and used the significant storm count of Figure 10 as a guideline for haboob frequency. For simplicity, we held fixed all parameters describing the haboob dust production (i.e., each observed storm produces an identical amount of total dust). Limitations of this assumption were reconciled in part by selecting a representative range of initial wind speeds and downdraft durations for these storms. For consistency, we assumed the same transportable fraction as the COAMPS™ simulation (10%), a reasonable step given that both models are based on the *Westphal et al.* [1987] source flux parameterization (equations (3)–(4)).

[77] Results of these simulations are presented in Figure 15, where the haboob dust production appears as a bracketed range of values based on assumptions of weaker (initial wind speeds of $U_0 = 20$ m/s) or stronger ($U_0 = 30$ m/s) systems. For most of the period, the haboob transportable dust contributions of 0.1–10 kilotons/day are small (at most only a few percent) compared to the total amounts lifted over the domain by the mesoscale to synoptic-scale forcing mechanisms resolved by COAMPS™, particularly during periods of widespread deflation (e.g., 10–15 September) when 24-hr totals exceeded 1 megaton. However, when haboob activity coincides with less pronounced synoptically forced dust activity (e.g., 15–25 September), the relative contributions from haboobs represent a significant (exceeding 30%) fraction of the daily regional dust production. These findings suggest the need for an improved and explicit account of downdraft deflation processes in transport and dispersion models, particularly for those regions where such activity is seasonally recurrent.

7. Conclusion

[78] Haboobs are as complex and poorly understood as they are visually impressive. Their sudden and isolated occurrence and transient impacts to the local environmental state make predicting and characterizing them quantitatively a formidable challenge. Given their profound short-term impacts on the local scale, and their potential to project long-term influences on regional scales, there is a growing awareness of our need to better understand and account for this special mechanism of deflation. The 2004 UAE^2 program provided a natural laboratory for the study of haboob formation and evolution within a prolific formation region, and a first opportunity to observe the events by a distributed network of meteorological stations, satellite, radar, and lidar coverage.

[79] In this study we have examined the haboob phenomenon from the perspectives of dynamics, thermodynamics, in situ and remote sensing observations, empirical parameterization, and idealized numerical modeling. Through an observation-oriented approach we illustrated haboob structure and evolution, evaluated previously reported techniques and metrics for downburst analysis (e.g., methods for estimating wind speed based on soundings, pressure jumps, cold pool temperature), and offered a simplified conceptual model for estimating haboob dust production. Even so, this work only begins to scratch the surface of the many considerations required to simulate haboob dust production realistically. Our hope here is to stimulate additional interest within the research community to advance this remarkably understudied topic in light of its relevance to both climatological research and immediate life/property impacts.

[80] The haboobs observed during UAE^2 were forced predominantly by dry microbursts, spawned by convective clouds which initiated at moist mid-levels and precipitated into a dry adiabatic lower atmosphere. The dust lifted by the gust fronts of these storms often traveled a significant distance (>100 km), consistent with previous reports that suggest their possible synoptic-scale influence. Whereas the dust front initially coincides with the cold pool front, it was found to lead the cold pool at increasing range from the source. In several cases, an environment favorable to

convective activity along the Al Hajar mountain range supported the near simultaneous formation of multiple storms. The ensuing production of concurrent downdrafts led to a complicated time history of haboob frontal passages throughout the domain, leading in turn to the initiation of new convection along colliding outflow boundaries. Sea breeze fronts, enhancement and cancellation by environmental flows, and superposition of storm motion further complicated the observed wind field and its evolution. Dynamic and thermodynamic properties of the convective downbursts themselves can result in rapidly fluctuating wind, temperature, and relative humidity fields even for a single, isolated event occurring under otherwise quiescent environmental conditions. Operators should be wary of the potential for ''back-side haboobs'' (propagating in a direction opposite to storm motion) when low-precipitation storms pass directly overhead or develop immediately downstream of their position.

[81] Statistically, the ensemble of haboob frontal passages collected over the August to September 2004 period produced 15-min mean wind speed increases of 10 m s^{-1}, pressure rises of 2 mb, humidity increases of 15%, and temperature drops of 7 °C. Satellite imagery revealed a distinct episodic nature of haboob activity over the eastern UAE domain (along the Al Hajar range), with convective activity clustering about multiday periods and peak storm count near the center of these clusters, suggesting an association with environmental conditions evolving along synoptic-weather timescales. The number of storms occurring within these clusters was also observed to increase toward the end of the two month study period. Inferred tendencies toward earlier convective initiation in later summer were less definitive due in part to the sample size (one partial season) and 30 min satellite temporal resolution. Until multiyear satellite analyses for this region are completed, these results must be considered as being very preliminary.

[82] To understand the relative importance of haboobs as a source for regional mineral aerosol and potential climate impacts, a physical model capable of computing the event-integrated total deflation under highly idealized conditions was developed. This model parameterized the space/time varying friction wind as a function of initial gust front wind speed and downdraft duration, based on observations taken from the UAE^2 case studies, and adopted the *Westphal et al.* [1987] source flux relationship. Comparing the haboob model total dust production against regionally integrated results from COAMPS™ over a half-month period suggested that there are occasions when enhanced haboob activity may account for a significant component of the regional transportable aerosol mass (e.g., up to one-third over a 1000 × 1000 km domain). As numerical weather prediction models continue to advance toward cloud resolving model scales and more sophisticated moist physics packages, an explicit account for deflation processes linked to convective downdrafts should become possible.

[83] Following the 2004 UAE^2 program, an abbreviated UAE-sponsored campaign focusing on aerosol-cloud indirect effects took place during the summer of 2006. Ground observations supporting this later effort included a portable met-station deployed atop a hotel in Al Ain, this time offering 1 min observations. Several haboobs were recorded over a ~4 week period, including one event that blew the met-station off the roof. Ongoing research will examine these higher time resolution single-station case studies. The optimal observing system for haboob measurement has yet to be realized, but would include (1) an evenly distributed (1 km grid) met-station network, (2) high temporal resolution (e.g., 30 s) met observations for gust front analysis, (3) surface radar/lidar network for volumetric dust/hydrometeor analysis, (4) particle probes for examining microphysics sedimentation and detecting nighttime events, (5) geostationary satellite observing systems providing rapid refresh (e.g., 1–5 min), high spatial resolution (e.g., 0.5 km visible, 1.0 km infrared), and a multispectral (e.g., MODIS-like) channel suite useful for dust detection and regional convection monitoring, and (6) opportunistic use of active spaceborne remote sensing systems (e.g., CloudSat cloud radar and CALIPSO 532 nm lidar) to provide vertical structure of convective clouds and dust-laden outflows. As in the western UAE, a ''mesonet'' deployed within a desert environment in close proximity to seasonal mid-level moisture influx and featuring a reliable orographic focus for convective initiation would provide the best opportunity for successful data gathering. Multiseason statistics collected in this fashion are needed to gain a full understanding of haboobs in the context of both their instantaneous and climatological impacts.

[84] **Acknowledgments.** We thank Stuart Piketh, Elizabeth A. Reid, Ahmed Habib, Tara Jensen, Piotr Flatau, and Steven Haddock for data and materials support, Dominik Brunner and Thierry Corti for software assistance, and Sebastian Engelstaedter, Tom Painter, and Fred Proctor for useful scientific discussions. The UAE^2 work was made possible through the significant logistical support of the UAE Office of his Highness the President, Department of Water Resources Studies (Now Department of Atmospheric Research). The support of our research sponsor, the Office of Naval Research under program element PE-0602435N, is gratefully acknowledged.

References

Ackerman, S. A. (1989), Using the radiative temperature difference at 3.7 and 11.0 μm to track dust outbreaks, *Remote Sens. Environ.*, *27*, 129–133.

Albrecht, B. (1989), Aerosols, cloud microphysics and fractional cloudiness, *Science*, *245*, 1227–1230.

Atkins, N. T., and R. M. Wakimoto (1991), Wet microburst activity over the southeastern United States: Implications for forecasting, *Weather Forecasting*, *6*, 470–482.

Babikir, A. A. A. (2004), Some aspects of climate and economic activities in the Arab Gulf States, *GeoJournal*, *13.3*, 211–222.

Bernardet, L. R., L. D. Grasso, J. E. Nachamkin, C. A. Finley, and W. R. Cotton (2000), Simulating convective events using a high-resolution mesoscale model, *J. Geophys. Res.*, *105*(D11), 14,963–14,982.

Bolton, D. (1980), The computation of equivalent potential temperature, *Mon. Weather Rev.*, *108*, 1046–1053.

Braham, R. R. (1952), The water energy budgets of the thunderstorm and their relation to thunderstorm development, *J. Meteorol.*, *9*, 227–242.

Brown, J. M., K. R. Knupp, and F. Caracena (1982), Destructive winds from shallow, high-based cumulonimbi, paper presented at 12th Conference on Severe Local Storms, Am. Meteorol. Soc., San Antonio, Tex.

Caracena, F., and M. W. Maier (1987), Analysis of a microburst in the FACE meteorological mesonetwork in southern Florida, *Mon. Weather Rev.*, *115*, 969–985.

Caracena, F., J. McCarthy, and J. A. Flueck (1983), Forecasting the likelihood of microbursts along the Front Range of Colorado, paper presented at 13th Conference on Severe Local Storms, Am. Meteorol. Soc., Tulsa, Okla.

Chen, W., and D. W. Fryrear (2002), Sedimentary characteristics of a haboob dust storm, *Atmos. Res.*, *61*, 75–85.

Clark, T. L., and R. List (1971), Dynamics of a falling particle zone, *J. Atmos. Sci.*, *28*, 718–727.

DeFries, R. S., and J. R. G. Townshend (1994), NDVI-derived land cover classification at a global scale, *Int. J. Remote Sens.*, *15*, 3567–3586.
d'Entremont, R. P., and L. W. Thomason (1987), Interpreting meteorological satellite images using a color composite technique, *Bull. Am. Meteorol. Soc.*, *68*, 762–768.
Emanuel, K. (1981), A similarity theory for unsaturated downdrafts within clouds, *J. Atmos. Sci.*, *38*, 1541–1557.
Flanner, M. G., and C. S. Zender (2006), Linking snowpack microphysics and albedo evolution, *J. Geophys. Res.*, *111*, D12208, doi:10.1029/2005JD006834.
Fujita, T. T. (1976), Spearhead echo and downburst near the approach end of a John F. Kennedy Airport runway, New York City, *SMRP 137*, 51 pp., Satell. and Mesometeorol. Res. Proj., Dept. of Geophys. Sci., Univ. of Chicago, Chicago, Ill.
Fujita, T. T. (1978), Manual of downburst identification for Project NIMROD, *SMRP Res. Pap. 156*, 104 pp., Univ. of Chicago, Chicago, Ill.
Fujita, T. T., and R. M. Wakimoto (1983), JAWS microbursts revealed by triple-Doppler radar, aircraft, and PAM data, paper presented at 13th Conference on Severe Local Storms, Am. Meteorol. Soc., Tulsa, Okla.
Giles, J. (2005), Climate science: The dustiest place on Earth, *Nature*, *434*, 816–819.
Gillette, D. A., and R. Passi (1988), Modeling dust emission caused by wind erosion, *J. Geophys. Res.*, *93*, 14,233–14,242.
Gillette, D. A., J. Adams, E. Endo, and D. Smith (1981), Threshold velocities for input of soil particles into the air by desert soils, *J. Geophys. Res.*, *85*, 5621–5630.
Gillies, J. A., W. G. Nickling, and G. H. McTainsh (1996), Dust concentrations and particle-size characteristics of an intense dust haze event: Inland Delta Region, Mali, West Africa, *Atmos. Environ.*, *30*(7), 1081–1090.
Ginoux, P., M. Chin, I. Tegen, J. Prospero, B. Holben, O. Dubovik, and S. J. Lin (2001), Sources and distributions of dust aerosols simulated with the GOCART model, *J. Geophys. Res.*, *106*, 20,255–20,273.
Gurka, J. J. (1977), The February 23–24 dust storm as viewed from GOES-1, *Satell. Appl. Inf. Note 77/6*, p. 2, U. S. Dep. of Commerce, Natl. Weather Serv., Washington, D. C.
Helgren, D. M., and J. M. Prospero (1987), Wind velocities associated with dust deflation events in the Western Sahara, *J. Clim. Appl. Meteorol.*, *26*, 1147–1151.
Hjelmfelt, M. R. (1987), The microbursts of 22 June 1982 in JAWS, *J. Atmos. Sci.*, *44*(12), 1646–1665.
Hodur, R. M. (1997), The Naval Research Laboratory's Coupled Ocean/Atmosphere Mesoscale Prediction System (COAMPS), *Mon. Weather Rev.*, *125*, 1414–1430.
Hogan, T. F., and T. E. Rosmond (1991), The description of the Navy operational global atmospheric prediction system's spectral forecast model, *Mon. Weather. Rev.*, *119*, 1786–1815.
Holben, B. N., et al. (2001), An emerging ground-based aerosol climatology: Aerosol Optical Depth from AERONET, *J. Geophys. Res.*, *106*, 12,067–12,097.
Idso, S. B., R. S. Ingram, and J. M. Pritchard (1972), An American haboob, *Bull. Am. Meteorol. Soc.*, *53*, 930–935.
Isidora, J., and W. A. Gallus Jr. (2004), MCS rainfall forecast accuracy as a function of large-scale forcing Weather Forecasting, , *19*(2), 428–439.
Kamburova, P. L., and F. H. Ludlam (1966), Rainfall evaporation in thunderstorm downdraughts, *Q. J. R. Meteorol. Soc.*, *92*, 510–518.
Knippertz, P., C. Deutscher, K. Kandler, T. Müller, O. Schulz, and L. Schütz (2007), Dust mobilization due to density currents in the Atlas region: Observations from the Saharan Mineral Dust Experiment 2006 field campaign, *J. Geophys. Res.*, *112*, D21109, doi:10.1029/2007JD008774.
Knupp, K. R. (1985), Precipitating convective cloud downdraft structure: A synthesis of observations and modeling, Ph.D. dissertation, 296 pp., Colo. State Univ., Boulder.
Krumm, W. R. (1954), On the cause of downdrafts from dry thunderstorms over the plateau area of the United States, *Bull. Am. Meteorol. Soc.*, *35*(3), 122–125.
Lawson, T. J. (1971), Haboob structure at Khartoum, *Weather*, *26*, 105–112.
Lee, T. F., F. J. Turk, and K. Richardson (1997), Stratus and fog products using GOES-8-9 3.9 μm data, *Weather Forecasting*, *12*, 664–677.
McCarthy, J., J. W. Wilson, and T. T. Fujita (1982), The Joint Airport Weather Studies Project, *Bull. Am. Meteorol. Soc.*, *63*(1), 15–22.
McCauley, J. F., C. S. Breed, M. J. Grolier, and D. J. MacKinnon (1981), The U. S. dust storm of February, 1977, in *Desert Dust: Origin, Characteristics, and Effect on Man*, edited by T. L. Pewe, *Spec. Pap. Geol. Soc. Am.*, *186*, 123–147.
Mctainsh, G., Y. Chan, H. McGowan, J. Leys, and K. Tews (2005), The 23rd October 2002 dust storm in eastern Australia: Characteristics and meteorological conditions, *Atmos. Environ.*, *39*, 1227–1236.
Membery, D. (1985), A gravity-wave haboob?, *Weather*, *40*(7), 214–221.
Miller, S. D. (2003), A consolidated technique for enhancing desert dust storms with MODIS, *Geophys. Res. Lett.*, *30*(20), 2071, doi:10.1029/2003GL018279.
Miller, S. D., T. F. Lee, F. J. Turk, A. P. Kuciauskas, and J. D. Hawkins (2005), Shedding new light on nocturnal monitoring of the environment with the VIIRS day/night band, *Proc. SPIE Int. Soc. Opt. Eng.*, *5890*, 201–209.
Miller, S. D., et al. (2006), MODIS provides a satellite focus on operation Iraqi Freedom, *Int. J. Remote Sens.*, *27*(7), 1285–1296, doi:10.1080/01431160500383772.
National Center for Atmospheric Research (2005), Final Report on the Rainfall Enhancement Assessment Program in the UAE (2001–2005), Natl. Cent. for Atmos. Res., Res. Appl. Lab., Boulder, Colo.
National Transportation Safety Board (1983), Aircraft accident report: Pan American World Airways, Inc., Clipper 759, Boeing 727-235, N4737, New Orleans International Airport, Kenner, Louisiana, 9 July 1982, 113 pp., *NTSB AAR-83/02*, Natl. Transp. Safety Board, Washington, D. C.
Newton, C. W. (1950), Structure and mechanism of the prefrontal squall line, *J. Meteorol.*, *7*(3), 210–222.
Orlanski, I. (1975), A rational subdivision of scales for atmospheric processes, *Bull. Am. Meteorol. Soc.*, *56*, 527–530.
Painter, T. H., A. P. Barrett, C. C. Landry, J. C. Neff, M. P. Cassidy, C. R. Lawrence, K. E. McBride, and G. L. Farmer (2007), Impact of disturbed desert soils on duration of mountain snow cover, *Geophys. Res. Lett.*, *34*, L12502, doi:10.1029/2007GL030284.
Pincus, R., and M. A. Baker (1994), Effect of precipitation on the albedo susceptibility of clouds in the marine boundary layer, *Nature*, *372*, 250–252.
Proctor, F. H. (1988), Numerical simulations of an isolated microburst. Part I: Dynamics and structure, *J. Atmos. Sci.*, *45*(21), 3137–3160.
Proctor, F. H. (1989), Numerical simulations of an isolated microburst. Part II: Sensitivity experiments, *J. Atmos. Sci.*, *46*(14), 2143–2165.
Prospero, J. M. (1999), Long-term measurements of the transport of African mineral dust to the southeastern United States: Implications for regional air quality, *J. Geophys. Res.*, *104*, 15,917–15,927.
Prospero, J. M., and R. T. Nees (1986), Impact of the North African drought and El Niño on mineral dust in the Barbados trade winds, *Nature*, *320*, 735–738.
Prospero, J. M., P. Ginoux, O. Torres, S. E. Nicholson, and T. E. Gill (2002), Environmental characterization of global sources of atmospheric soil dust identified with the NIMBUS 7 Total Ozone Mapping Spectrometer (TOMS) absorbing aerosol product, *Rev. Geophys.*, *40*(1), 1002, doi:10.1029/2000RG000095.
Riley, J. A. (1931), Sandstorms in Texas, *Mon. Weather Rev.*, *59*, 30–31.
Rodi, A. R., K. L. Elmore, and W. P. Mahoney (1983), Aircraft and Doppler air motion comparisons in a JAWS microburst, paper presented at the 21st Conference on Radar Meteorology, Am. Meteorol. Soc., Edmonton, Canada.
Simpson, J. E. (1969), A comparison between laboratory and atmospheric density currents, *Q. J. R. Meteorol. Soc.*, *95*, 758–765.
Sokolik, I. N., and O. B. Toon (1996), Direct radiative forcing by anthropogenic mineral aerosols, *Nature*, *381*, 681–683.
Sokolik, I. N., O. B. Toon, and R. W. Bergstrom (1998), Modeling the radiative characteristics of airborne mineral aerosols at infrared wavelengths, *J. Geophys. Res.*, *103*, 8813–8826.
Spinhirne, J. D., J. Rall, and V. S. Scott (1995), Compact eye-safe lidar systems, *Rev. Laser Eng.*, *23*, 26–32.
Squires, P. (1958), Penetrative downdraughts in cumuli, *Tellus*, *10*, 381–389.
Srivastava, R. C. (1985), A simple model of evaporatively driven downdraft: Application to microburst downdraft, *J. Atmos. Sci.*, *42*(10), 1004–1023.
Sutton, I. I. (1925), Haboos, *Q. J. R. Meteorol. Soc.*, *51*, 25–50.
Twomey, S. (1974), Pollution and the planetary albedo, *Atmos. Environ.*, *8*, 1251–1256.
Uno, I., et al. (2006), Dust model intercomparison (DMIP) study over Asia: Overview, *J. Geophys. Res.*, *111*, D12213, doi:10.1029/2005JD006575.
Vogel, B., C. Hoose, H. Vogel, and C. Kottmeier (2006), A model of dust transport applied to the Dead Sea area, *Meteorol. Z.*, *15*(6), 611–624.
Wakimoto, R. M. (1983), The West Bend, Wisconsin storm of 4 April 1981: A problem in operational meteorology, *J. Clim. Appl. Meteorol.*, *22*, 181–189.
Wakimoto, R. M. (1985), Forecasting dry microburst activity over the High Plains, *Mon. Weather Rev.*, *113*, 1131–1143.
Wakimoto, R. M., and V. N. Bringi (1988), Dual-polarization observations of microbursts associated with intense convection: The 20 July storm during the MIST project, *Mon. Weather Rev.*, *116*, 1521–1539.
Weisman, M. L., J. B. Klemp, and J. W. Wilson (1983), Dynamic interpretation of notches, WERS, and mesocyclones simulated in a numerical

cloud model, paper presented at 21st Conference on Radar Meteorology, Am. Meteorol. Soc., Edmonton, Canada.

Welton, E. J., J. R. Campbell, J. D. Spinhirne, and V. S. Scott (2001), Global monitoring of clouds and aerosols using a network of micro-pulse lidar systems, in *Lidar Remote Sensing for Industry and Environmental Monitoring*, edited by U. N. Singh et al., *Proc. SPIE Int. Soc. Opt. Eng.*, *4153*, 151–158.

Westphal, D. L., O. B. Toon, and T. N. Carlson (1987), A two-dimensional numerical investigation of the dynamics and microphysics of Saharan dust storms, *J. Geophys. Res.*, *92*, 3027–3049.

Westphal, D. L., O. B. Toon, and T. N. Carlson (1988), A case study of mobilization and transport of Saharan dust, *J. Atmos. Sci.*, *45*, 2145–2175.

Williams, E., N. Nathou, E. Hicks, C. Pontikis, B. Russell, M. Miller, and M. J. Bartholomew (2007), The electrification of dust-lofting gust fronts ('haboobs') in the Sahel, paper PS3-17 presented at 13th International Conference on Atmospheric Electricty, Chin. Acad. of Sci., Beijing, 13–17 Aug.

Wilson, J., C. Kessinger, and J. McCarthy (1984), Microburst wind structure and evaluation of Doppler radar for airport wind shear detection, *J. Clim. Appl. Meteorol.*, *23*, 898–915.

Wolfson, M. (1983), Doppler radar observations of an Oklahoma downburst, paper presented at 21st Conference on Radar Meteorology, Am. Meteorol. Soc., Edmonton, Canada.

D. W. Breed, National Center for Atmospheric Research, Boulder, CO 80307, USA.

Q. Ji, Earth System Science Interdisciplinary Center, University of Maryland, College Park, MD 20742, USA.

A. P. Kuciauskas, M. Liu, J. S. Reid, and A. L. Walker, Satellite Meteorological Applications Section, Marine Meteorology Division, Naval Research Laboratory, 7 Grace Hopper Avenue, MS#2, Monterey, CA 93943-5502, USA. (miller@nrlmry.navy.mil)

A. A. Mandoos, Department of Atmospheric Studies, Ministry of Presidential Affairs, P.O. Box 4815, Abu Dhabi, United Arab Emirates.

S. D. Miller, Cooperative Institute for Research in the Atmosphere (CIRA), Colorado State University – Foothills Campus, 1375 Campus Delivery, Fort Collins, CO 80523, USA. (miller@cira.colostate.edu)